the plant journal

SEB SOCIETY FOR EXPERIMENTAL BIOLOGY

The Plant Journal (2025) **121,** e17259 doi: 10.1111/tpj.17259

RESOURCE

Defining the heterogeneous composition of Arabidopsis thylakoid membrane

Andrea Trotta[1,2,*,†], Sanna Gunell[1,†], Azfar Ali Bajwa[1], Virpi Paakkarinen[1], Hiroaki Fujii[1] and Eva-Mari Aro[1,*]

[1]*Molecular Plant Biology, Department of Life Technologies, University of Turku, Turku FIN-20014, Finland, and*

[2]*Institute of Bioscience and BioResources (IBBR), National Research Council of Italy (CNR), via Madonna del Piano, 10, Sesto Fiorentino, Firenze 50019, Italy*

Received 4 September 2024; revised 28 November 2024; accepted 18 December 2024.

*For correspondence (e-mail andrea.trotta@cnr.it and evaaro@utu.fi).

†These authors contributed equally to this work.

SUMMARY

Thylakoid membrane (TM) of land plants is organized into an appressed domain (grana), enriched in photosystem (PS) II and a non-appressed domain (stroma lamellae) enriched in PSI. This ultrastructure controls the exciton spillover from PSII to PSI. The bulky machinery required for the biogenesis and repair of TM protein complexes is located in the non-appressed membranes. Thus, the connecting domain (CD) between grana and stroma lamellae is the key player in both the structural and functional integrity of the photosynthetic machinery. In addition, both the grana domain and the stroma lamellae are highly curved at their edges due to the action of the CURVATURE1 (CURT1) proteins, forming a domain distinct from the CD, called the curvature. Here we elucidate the biochemical properties and proteome composition of different thylakoid domains. To this end, the TM of *Arabidopsis thaliana* (Arabidopsis), isolated both in the natural stacked configuration and in an artificially unstacked configuration to induce a homogeneous protein composition, was solubilized and fractionated, using the mild detergent digitonin (DIG). Using mass spectrometry-based proteomics, we characterize composition, distribution and interaction of proteins involved in TM function in grana, CD and stroma lamellae domains. We find that a subset of thylakoid protein complexes are readily solubilized into small vesicles by DIG and accumulate in a loose pellet (LP) together with CURT1. By combining an extensive biochemical and proteome characterization of the TM fractions we provide an optimized protocol and proteome maps that can be used as a basis for experimental design in photosynthesis research.

Keywords: *Arabidopsis thaliana*, thylakoid proteomics, thylakoid ultrastructure, thylakoid domains, digitonin solubilization.

INTRODUCTION

The thylakoid membrane (TM) of land plant chloroplasts houses the photosynthetic machinery capable of light-driven oxidation of water in photosystem (PS) II and subsequent reduction of $NADP^+$ by PSI, with concomitant generation of a proton gradient across the TM for production of ATP. The major protein complexes, PSII, PSI, light-harvesting complex (LHC) I and II, Cytochrome (Cyt) b_6f and ATP synthase are heterogeneously distributed between the two main domains of the TM: the appressed (stacked) grana membranes and the non-appressed stroma-exposed membranes (SEM). This organization, among other things, controls the spillover of excitons from PSII to PSI, which are mainly located in the appressed stacked membranes and the non-appressed SEM, respectively (Anderson, 2012; Anderson et al., 2012; Andersson & Anderson, 1980). Grana are organized as stacked discs surrounded by right-handed helices of stroma lamellae (SL) which in turn are connected to grana membranes by several fret-like structures per disc (Bussi et al., 2019), defined here as connecting domains (CD). The flat TM sacks end with highly curved stroma-exposed structures, defined here as curvature domains (Figure 1a). This domain is found at the periphery of all grana discs (Daum & Kuhlbrandt, 2011; Rantala et al., 2020; Raven, 2021), but also at the periphery of the SL and wherever the TM sacks

are highly curved, such as the aqueous conduits for diffusion of stromal proteins formed by the left-handed helical structures observed in the SL (Bussi et al., 2019). The three domains, SL, CD and curvature, together with the end membranes on the grana disks (Figure 1a), form the SEM.

Advances in electron tomography have definitively shown that the periphery of the same grana disc is formed

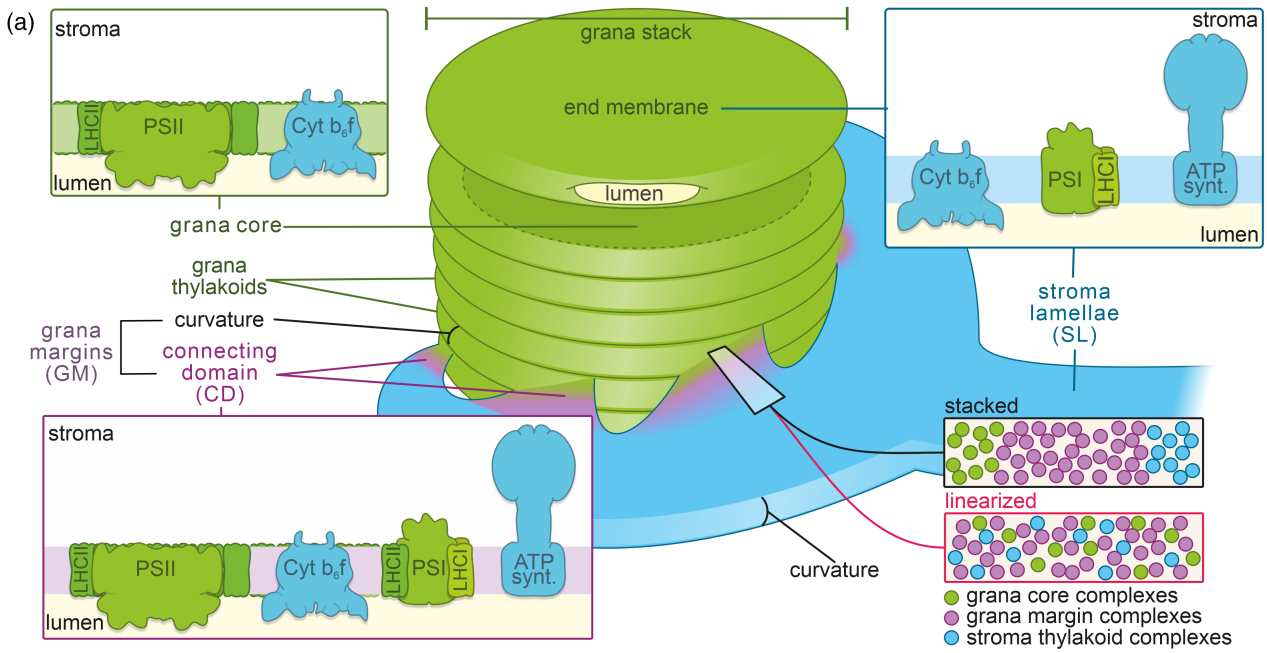

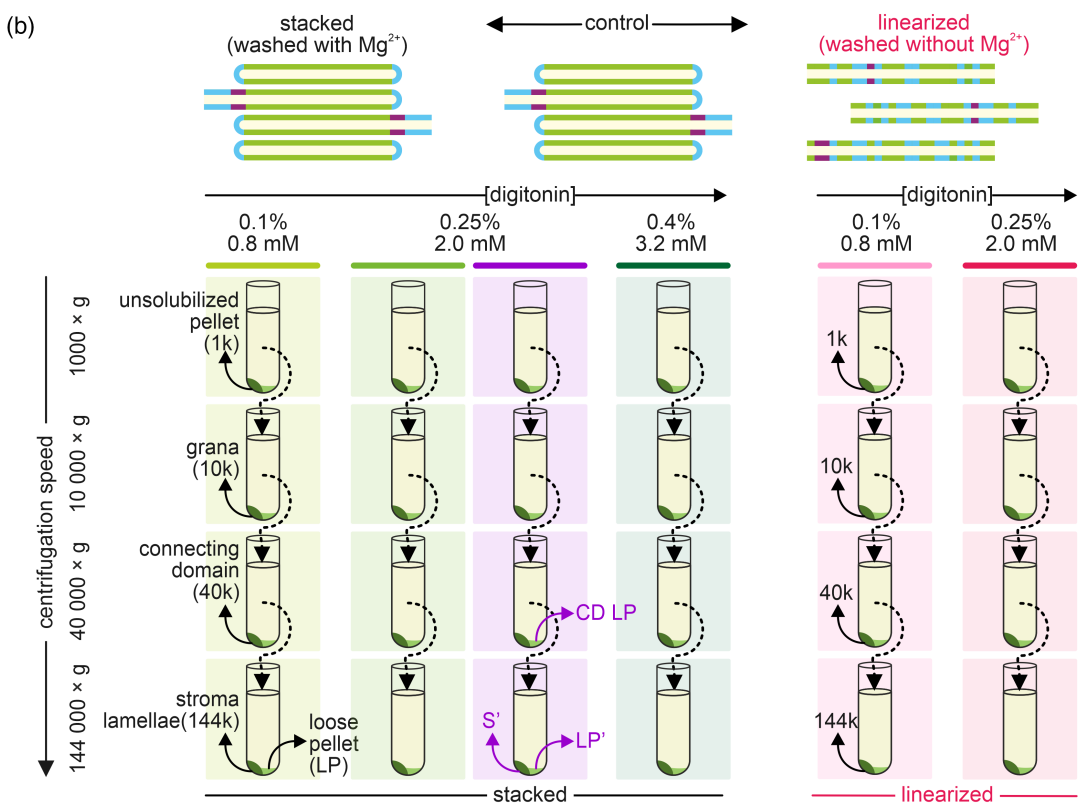

Figure 1. Thylakoid membrane (TM) model and experimental procedure.
(a) Simplified scheme of the interconnections between appressed and non-appressed domains of the TM, represented as one granum (green discs) connected by fret-like structures (connecting domains, CD, purple) to one stroma lamella (SL, light blue) wrapping around the granum in a right-handed fashion. A fourth domain, the curvature, is present at the periphery of each grana disc, where the disc is not connected to SL via CD, and in any other place of the TM where the bilayer is highly curved. The CD and curvature domains are collectively called as grana margin (GM), due to historical reasons (see Introduction). The grana core is enriched in PSII-LHCII, while the stroma thylakoid is enriched in PSI-LHCI. CD hosts both photosystems and the PSI-LHCII complex. ATP synthase is present in all stroma-exposed membranes (SEM), while Cyt b6f is roughly equally present in grana core, CD and SL. The membranes of the upper most and lower most grana discs directly exposed to stroma (end membranes) have the same composition of SL. In the proposed model, the strict heterogeneity in intact TM (magnification box in the right bottom corner) is lost upon TM linearization and, consequently, the micro-domains of grana core, CD and SL get mixed.
(b) Experimental procedure to isolate different TM domains and to dissect the interaction of the detergent digitonin (DIG) with the TM protein complexes. Isolated intact TMs (control) were washed six times in the presence (stacked) or absence (linearized) of Mg^{2+}, followed by solubilization with several different [DIG]. Each [DIG]-solubilized TM was then fractionated with increasing centrifugation speed into unsolubilized pellet (1000 ***g***, 1k ***g***), grana (10k), connecting domain (40k) and stroma lamellae (144k). A loose pellet (LP), containing the curvature, was also harvested at 144k. The color coding on the top of each column, indicating both the [DIG] used and the TM status (stacked or linearized), are the same in all figures to help the orientation of the reader when examining other figures.

by alternating domains of curvature and CD (Bussi et al., 2019; Daum & Kuhlbrandt, 2011). Biochemical TM fractionation, however, has generally made no distinction between these two structural domains (curvature and CD in frets) and they have been collectively referred to as grana margins (GM) (Figure 1a). In fact, the definition and composition of the GM has long been debated with no broad consensus reached (Anderson, 2012; Dekker & Boekema, 2005; Mazur et al., 2021; Rantala et al., 2020; Raven, 2021). Historically, the GM has been defined as the protein-free, highly curved domains at the periphery of the grana discs (Dekker & Boekema, 2005; Murphy, 1986), which cannot accommodate large membrane-spanning protein complexes, according to initial cryo-EM and tomography studies (Anderson et al., 2012; Daum et al., 2010). However, parallel research based on mechanical TM fractionation assigned a specific TM domain also as a GM, which instead contained large protein complexes (Danielsson & Albertsson, 2009; Wollenberger et al., 1994). Such a GM cannot coincide with the highly curved region (curvature, Figure 1a) at the periphery of the grana discs, due to both the steric hindrance of the large protein complexes and the lack of continuity with the stroma lamellae, where the ribosomes and the rest of the translation machinery can be located (Yamamoto et al., 1981). To avoid these nomenclature problems, we have marked GM in Figure 1(a) to contain both the curvature and the connecting (CD) domains. The CD represents a site where the assembly and repair machinery are closest to the final location of their substrates (i.e., PSII, LHCII and Cyt b_6f), and can be defined as the functional domain of the GM (Järvi et al., 2015; Rantala et al., 2020). One of the best functional examples in CD is the PSII repair cycle: upon photodamage to the D1 protein of PSII in the grana core, the PSII-LHCII complexes are disassembled and the PSII monomer gains access to the CD, where a new copy of D1 is co-translationally inserted into the CP43-less PSII monomer (hereafter: CP43-less) (Järvi et al., 2015; Lu, 2016; Theis & Schroda, 2016; Zhang et al., 2000).

In grana stacks, the strong curvature of the grana discs is maintained by the action of the CURT1 proteins (Armbruster et al., 2013) (Figure 1a, curvature domain). The CURT1 containing curvature domain was isolated by detergent-based fractionation of the TM, using the sterol-based saponin digitonin (DIG) (Koochak et al., 2019; Puthiyaveetil et al., 2014; Trotta et al., 2019), or the synthetic glycodiosgenin (Maeda et al., 2022; Nishioka et al., 2021). Sterol-containing detergents such as DIG, cholate and CHAPS have been instrumental in the isolation and purification of thylakoid protein complexes such as ATP synthase and Cyt b_6f (Hurt & Hauska, 1981; Nelson & Neumann, 1972; Pick & Racker, 1979). Due to the weak interaction of sterol-based detergents with cholesterol-poor biological membranes (Fan & Heerklotz, 2017; Sudji et al., 2015), their effect on the solubilization of specific protein complexes is not fully understood. Nevertheless, the use of DIG in the pioneering work of Emil Smith initially led to the discovery of thylakoid domains enriched in PSII and PSI activities (Smith, 1988 and references therein). Subsequently, the application of ultracentrifugation steps at increasing speeds (10 000 ***g*** [10k], 40 000 ***g*** [40k] and 144 000 ***g*** [144k]) allowed the separation of TM fractions characterized by increasing chlorophyll (chl) *a*/*b* ratios, from PSII-LHCII enriched appressed membranes via CD to PSI enriched in SL (Anderson & Boardman, 1966; Anderson & Vernon, 1967). The loss of lateral heterogeneity of the TM, achieved by depletion of Mg^{2+} and K^{+} which leads to unstacking of the appressed domains, results in a similar chl *a*/*b* ratio of the light (144k), medium (40k) and heavy (10k) fractions (Anderson & Vernon, 1967). This is consistent with the randomization of the protein complexes after linearization of the TM, resulting in the spillover of excitation energy from PSII to PSI (Anderson & Vernon, 1967; van der Weij-de Wit et al., 2007). The protocol for the separation of the 10k, 40k and 144k fractions, which are assumed to be enriched in grana core, CD and SL, respectively, has been widely used by researchers based on the experimental design developed by Kyle et al. (1984). The 40k fraction was defined as CD by (Kettunen et al., 1992; Rantala et al., 2020) because it has an intermediate protein composition and chl *a*/*b* ratio

with respect to 10k and 144k, similar to a fraction obtained after TM sonication and fractionation by two-phase partitioning (Danielsson et al., 2006; Wollenberger et al., 1994). However, several recent publications have collected the CD and the grana core together in a single step at 40k.

Although the structural details of the TM architecture can be conveniently studied by electron tomography, this technique does not provide details on the distribution and localization of most proteins and protein complexes in different TM domains. For this purpose, the best approach would be to apply proteomics to the vesicles obtained by mechanical fractionation of the TM, but unfortunately this method has not been successful in Arabidopsis, which has one of the best annotated genome databases among the model plant species. On the other hand, the enrichment of proteins and protein complexes in different TM domains by detergent fractionation, the most popular fractionation method, is prone to contamination due to the fusogenicity of membrane vesicles (Dlouhý et al., 2021) and various interactions between detergents and lipid microdomains surrounding the membrane protein complexes, which must be considered when interpreting the results.

In this work, we have thoroughly investigated the lateral heterogeneity and domain composition of the TM using the DIG solubilization followed by the differential centrifugation method. We have paid particular attention to the distinction between the TM 'curvature' and the TM 'connecting domain' (CD) (collectively referred to here as the grana margin, GM, for historical reasons – see above) in terms of their functional role and location in the laterally heterogeneous TM. Our results provide an explanation for the puzzling solubilization of protein complexes such as Cyt b_6f or PSII monomer complexes. Furthermore, we provide a detailed map of the distribution of more than 800 proteins in the fractions isolated by an optimized protocol using DIG. This database will not only highlight the specific functional role of the CD, but will also serve as a reference for plant scientists to localize their proteins of interest in the widely used DIG-based fractionation protocol of TM.

RESULTS

Overall pattern of pigment protein complexes from stacked and linearized TMs

Since thylakoid stacking is a native property to segregate the pigment-protein complexes into different TM domains, we first evaluated the overall composition of TM protein complexes in light-acclimated Arabidopsis plants grown under a low light intensity (see "Materials and Methods" section), both directly after TM isolation (control) and after repeated washes in the presence (stacked) or absence (linearized) of $MgCl_2$ (Figure 1b), followed by TM solubilization with 1% DIG or 1% β-dodecyl-*n*-maltoside (β-DM) and separation of the protein complexes by lpBN-PAGE (Figure 2a). Despite the presence of the same protein complexes in these three TM preparations, the DIG solubilization quantitatively revealed a higher abundance of PSII monomer, as well as L-LHCII and M-LHCII (Rantala et al., 2020), in linearized thylakoids compared to stacked thylakoids (Figure 2a, first three lanes). On the other hand, β-DM solubilized thylakoids were largely depleted of PSII-LHCII supercomplexes (sc) in linearized TM compared to stacked TM (Figure 2a, last three lanes). Notably, the PSI-LHCII complex, present only in DIG solubilized TM, was not appreciably affected by thylakoid linearization, in agreement with previous reports based on analysis of the fluorescence emission spectra at 77 K (van der Weij-de Wit et al., 2007).

Subfractionation of linearized and stacked thylakoids produces different patterns of protein complexes

Stacked and linearized thylakoid preparations were then subjected to fractionation using 0.25% DIG solubilization to examine the separation of thylakoid proteins (complexes). This [DIG] was lower than generally used in previous reports (Kyle et al., 1984; Trotta et al., 2019), due to the fact that the purity of the CURT1-containing fraction increases by decreasing [DIG] (Trotta et al., 2019). Here, in addition to the strong pellets obtained after centrifugation steps at

Figure 2. Analysis of thylakoid membrane (TM) protein complexes and their interaction in stacked and linearized TM.
(a) Representative lpBN-PAGE of TM protein complexes solubilized with either 1% DIG or 1% β-DM (at Chl concentration of 0.25 mg ml^{-1}). Solubilization was performed for non-washed TM (control) and after several washings in the presence or absence of Mg^{2+} (stacked and linearized TM, respectively), the volume corresponding to 5 μg of chl was loaded per lane. The major protein complexes are indicated next to the gels.
(b) Separation in lpBN-PAGE of the protein complexes fractionated from stacked (left) and linearized (right) thylakoids. Before fractionation, the thylakoids were solubilized with 0.25% DIG and then fractionated by centrifugation to 10k ***g***, 40k and 144k strong pellets and to the LP at 144k. For loading on the gel, all pelleted fractions and LP from stacked and linearized thylakoids were solubilized with 1% DIG and volumes equivalent to 5 μg of chl were loaded on each well. The chl *a*/*b* ratio of each sample is indicated at the bottom of each lane. Lane T indicates intact thylakoids. The major protein complexes are indicated next to the gel. A PSI supercomplex (PSI sc), corresponding to a PSI dimeric complex, visible in 2D BN/SDS-PAGE in Figure S2, is indicated in 40k and 144k fractions. PSI-LHCII complex is indicated by blue arrows.
(c) Separation in lpBN-PAGE of the protein complexes from the fractions obtained at 1k ***g***, 10k, 40k, 144k and the LP at 144k, after solubilization of thylakoids with 0.25% DIG from stacked (left) and linearized (right) thylakoids. Before loading on the wells (5 μg of chl per lane), each sample was solubilized with 1% β-DM. The major protein complexes are indicated next to the gels. A PSI supercomplex (PSI sc), corresponding to a PSI dimeric complex is indicated as in (b).
(d) Fluorescence emission spectra recorded at 77 K from stacked (light green) and linearized (pink) intact thylakoids (T), and from the corresponding fractions obtained from stacked and linearized T at 1k ***g***, 10k, 40k, 144k and the LP at 144k after solubilization with 0.25% DIG. The peaks at 680 nm corresponding to detached LHCII, at 685 nm to PSII subunit CP47, at 695 nm to PSII subunit CP43 and at 733 nm to PSI are highlighted by vertical lines throughout the graphs.

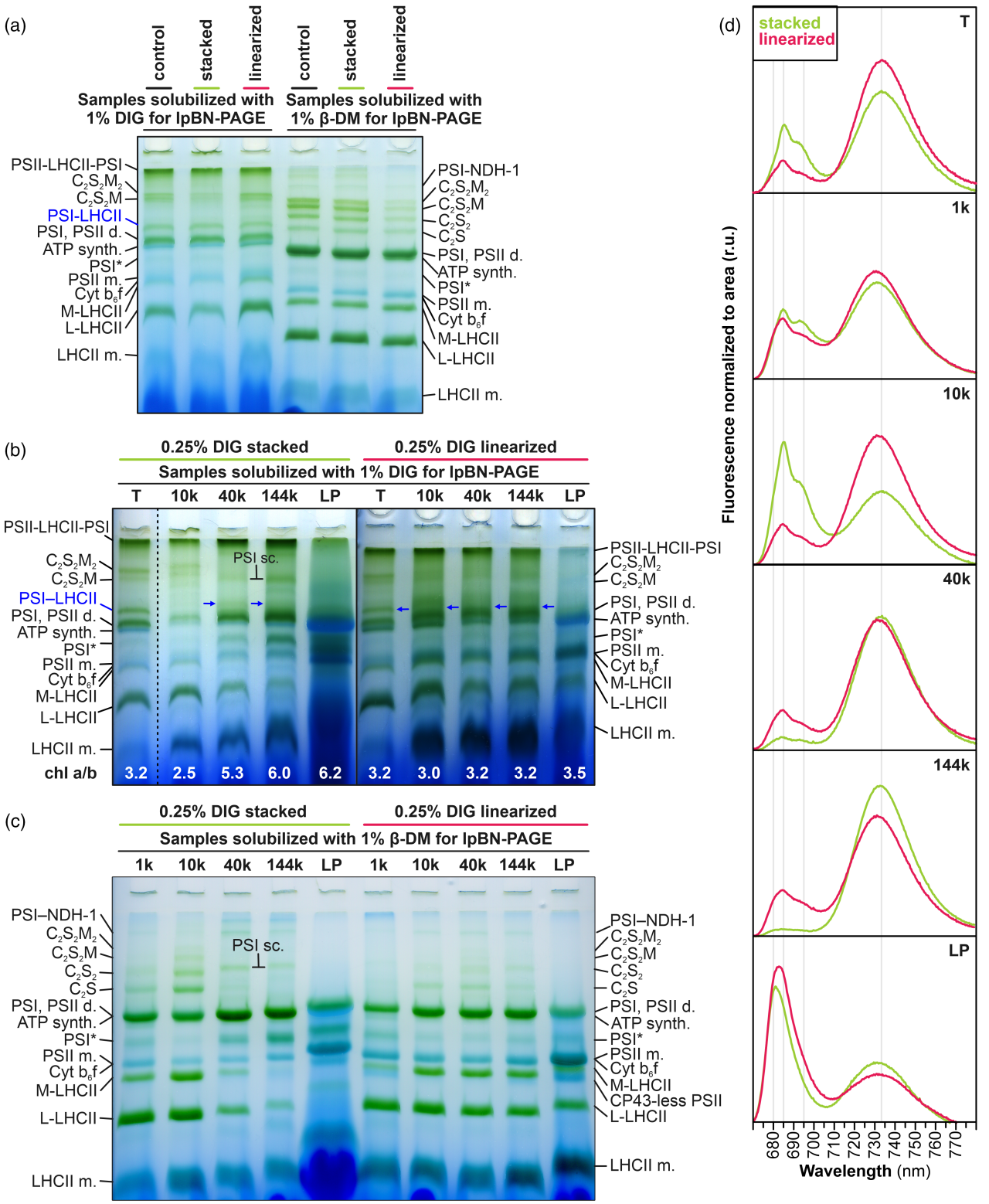

1000 ***g*** (unsolubilized thylakoid pellet, or 1k), 10k (grana core), 40k (connecting domain, CD) and 144k (stroma lamellae, SL), a loose pellet (LP) was also collected at 144k (Figures 1b and 2; Figure S1, see below).

The chl *a*/*b* ratio of the different fractions obtained from linearized thylakoids hardly differed from each other, ranging between 3.0 and 3.2, close to that of intact stacked thylakoids (Figure 2b, bottom of the lpBN-PAGE), due to

the homogeneous redistribution of PSII-LHCII and PSI-LHCI complexes along the linearized TM (Figure 2). Instead, a classical increase from 2.5 (10k fraction) to 5.3 and 6.0 (40k and 144k fractions, respectively) (Kyle et al., 1984; Trotta et al., 2019) was observed in the corresponding fractions from stacked thylakoids (Figure 2b), indicating strong lateral heterogeneity of PSII, LHC and PSI.

Consistently, the composition of protein complexes from linearized TM was very similar in 10k, 40k and 144k fractions, in contrast to the highly heterogeneous distribution in fractions from stacked TM of, for example, the PSII-LHCII, the M- and L-LHCII complexes, all of which were depleted in 40k and 144k fractions (Figure 2b,c; Figures S2 and S3). However, consistent with the chl *a*/*b* ratio, the 40k fraction from stacked TM contained M- and L-LHCII complexes to some extent, indicating that this fraction originated from SEM closer to grana with respect to 144k. Notably, the PSI-LHCII complex, which is highly visible in intact thylakoids, was partially lost during the fractionation procedure (Figure 2b; Figure S3). However, the highest percentage of residual PSI-LHCII was found in the 40k fraction (enriched in CD) of stacked thylakoids and, to a lesser extent, in the 144k fraction (enriched in SL) as well as in the 1k fraction (unsolubilized pellet) (Figure 2b and indicated by blue arrows in Figures S2 and S3).

As a consequence of TM linearization (Figure 2b; Figure S3), several PSI bands (PSI-LHCII complex, PSI* and PSI-LHCI, see blue arrows in Figure S3) were visible in the 10k fraction in addition to those in the 40k and 144k fractions. Distinct PSII-LHCII sc were also visible in the strong pellets from linearized thylakoids, probably corresponding to C2S, C2S2 and C2SM complexes (Caffarri et al., 2009) (Figure S3). Notably, the PSI-LHCII complex was not visible in the LP fractions from either linearized or stacked thylakoids (Figure 2b; Figure S3) (see below).

Structural analysis of the TM subfractions

Characterization of the fractions obtained with 0.25% DIG by transmission electron microscopy (TEM) revealed the presence of vesicles of similar shape but different size in the 10k, 40k and 144k fractions of linearized TM (Figure 3; Figure S4). Higher magnification showed the possible presence of ATP synthase in all fractions from linearized TM, confirming the randomization of protein complexes (Figure 3). In contrast, the 10k fraction from stacked TM contained the highest percentage of largest vesicles (Figure S4), representing grana core as previously observed (Kouřil et al., 2013), while the 40k contained smaller vesicles, which were often bent, and the 144k contained even smaller vesicles (Figure S4), which, in contrast to 10k and 40k, showed the presence of ATP synthase complexes (Figure 3).

The fluorescence emission spectra recorded at 77 K were almost identical in all strong pellets of linearized TM, and very similar to those of the corresponding intact linearized TM (Figure 2d). Conversely, the strong pellets from stacked TM showed an enrichment of the PSII signal (peaking at 685 and 695 nm) in 1k and 10k fractions, whereas the PSI signal (peaking at 733 nm) was enriched in 40k and 144k fractions (Figure 2d). These results (Figures 2 and 3) further confirmed that linearization of the TM leads to randomization of the chl-binding protein complexes and consequently to energy spillover from PSII to PSI (van der Weij-de Wit et al., 2007).

Effect of DIG concentration on separation of Cyt b_6f, ATP synthase and PSII subcomplexes in LP

In sharp contrast to the uniform distribution of protein complexes observed in the 10k, 40k and 144k fractions of linearized thylakoids, the corresponding LP showed marked differences, being particularly depleted in PSII-LHCII sc and PSI (Figure 2b,c; Figures S3 and S5). Furthermore, thylakoid linearization did not alter the strong accumulation of ATP synthase, PSII monomer, Cyt b_6f and CP43-less PSII in the LP fraction, which similarly characterized the LP obtained from stacked thylakoids (Figure 2b,c; Figures S3 and S5a). The 77 K fluorescence spectra of LPs showed a strong presence of PSII monomer (685 nm) and detached LHCII (680 nm), the latter being more prominent in LP from stacked TM (Figure 2d). The visualization with TEM of LP from stacked TM revealed a strong predominance of very small (<3000 nm^2) vesicles (Figure S4), many of which may contain ATP synthase (Figure 3). In contrast, the LP from linearized TM was a mixture of very small vesicles (<3000 nm^2) and larger vesicles (3000–11 750 nm^2), which could harbor the M- and L-LHCII complexes observed in BN-PAGE (Figure 2b,c; Figure S3b).

Semi-quantitative immunoblot analyses further confirmed that the distribution of PSI, PSII and LHCII in the 1k, 10k, 40k and 144k fractions from linearized thylakoids was more homogeneous along the TM compared to the corresponding fractions from stacked thylakoids (Figure 4a,b). However, the other major protein complexes, that is, Cyt b_6f and ATP synthase, together with the CURT1 proteins (CURT1A and 1B), were mostly concentrated in the LP from both the stacked and linearized thylakoids (Figure 4a,b). A similar differential separation was obtained by solubilizing the stacked thylakoids with 0.4% DIG (Figure 4a; Figure S5b). However, comparing the two LPs obtained with 0.4% and 0.25% DIG by 2D-lpBN/SDS-PAGE, it turned out that the relative abundance of CURT1 protein, PSII monomer, CP43-less, Cyt b_6f and ATP synthase was lower at 0.4% DIG (Figure 4c). Since SDS-PAGE is loaded on a chl basis, this effect is due to increased contamination/accumulation of chl-binding protein complexes such as PSI and LHCII in the LP upon use of higher [DIG] to solubilize thylakoids (see Trotta et al., 2019).

The above results regarding the LP fraction, are in apparent contradiction with the idea that linearization of

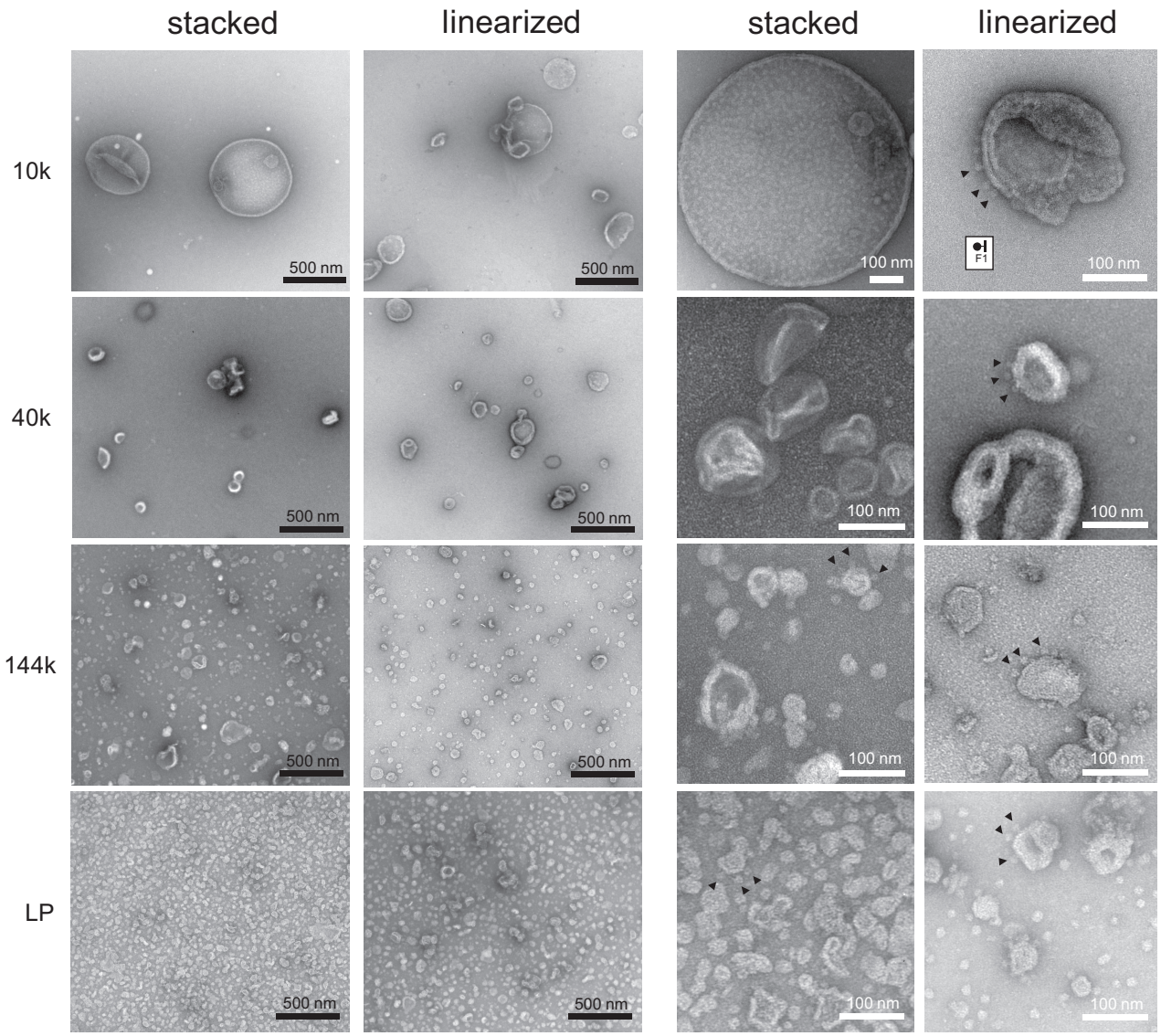

Figure 3. Analysis of thylakoid membrane (TM) fractions by transmission electron microscopy.
The stacked and linearized thylakoid fractions collected at 10k, 40k, 144k and LP (collected at 144k) were negatively stained and photographed with TEM. The same magnification pictures of all fractions (on the left two columns, scale bars: 500 nm) and higher magnification of featured structures in each fraction (on the right two columns, Scale bars: 100 nm) are shown. The average size of the F1 sector of spinach ATP synthase (Daum et al., 2010) is provided in the index. Arrowheads point to structures assigned as ATP synthases.

stacked TM leads to a uniform distribution of all protein complexes in all fractions or TM domains (Figure 1a) (Anderson & Vernon, 1967). These discrepancies suggest that the composition of the protein complexes in the LP fraction probably does not only reflect that of the curvature domain but is also influenced by specific interactions between DIG and the annular lipids of individual protein complexes, resulting in accumulation of specific protein complexes in the LP. The interaction of DIG with membranes such as cholesterol-free TM has been postulated to involve only the penetration of the outer leaflet of lipid bilayers. This results in the disruption of TM into smaller vesicles to re-equilibrate the asymmetric curvature created by the insertion of DIG molecules into one of the two layers (Figure 4d) (Fan & Heerklotz, 2017; Sudji et al., 2015). However, some TM protein complexes were clearly solubilized in DIG micelles, as indicated by the bands resolved in our BN-PAGE (Figures 2a,b and 4d) and by the small size of a part of the vesicles observed by TEM (Figure 3; Figure S4).

To visualize which protein complexes are easily solubilized by DIG, the stacked TM was solubilized with either 0.4% DIG or 1% DIG before loading on the BN-PAGE. As shown in Figure 5(a), the PSII monomer, Cyt b_6f and ATP

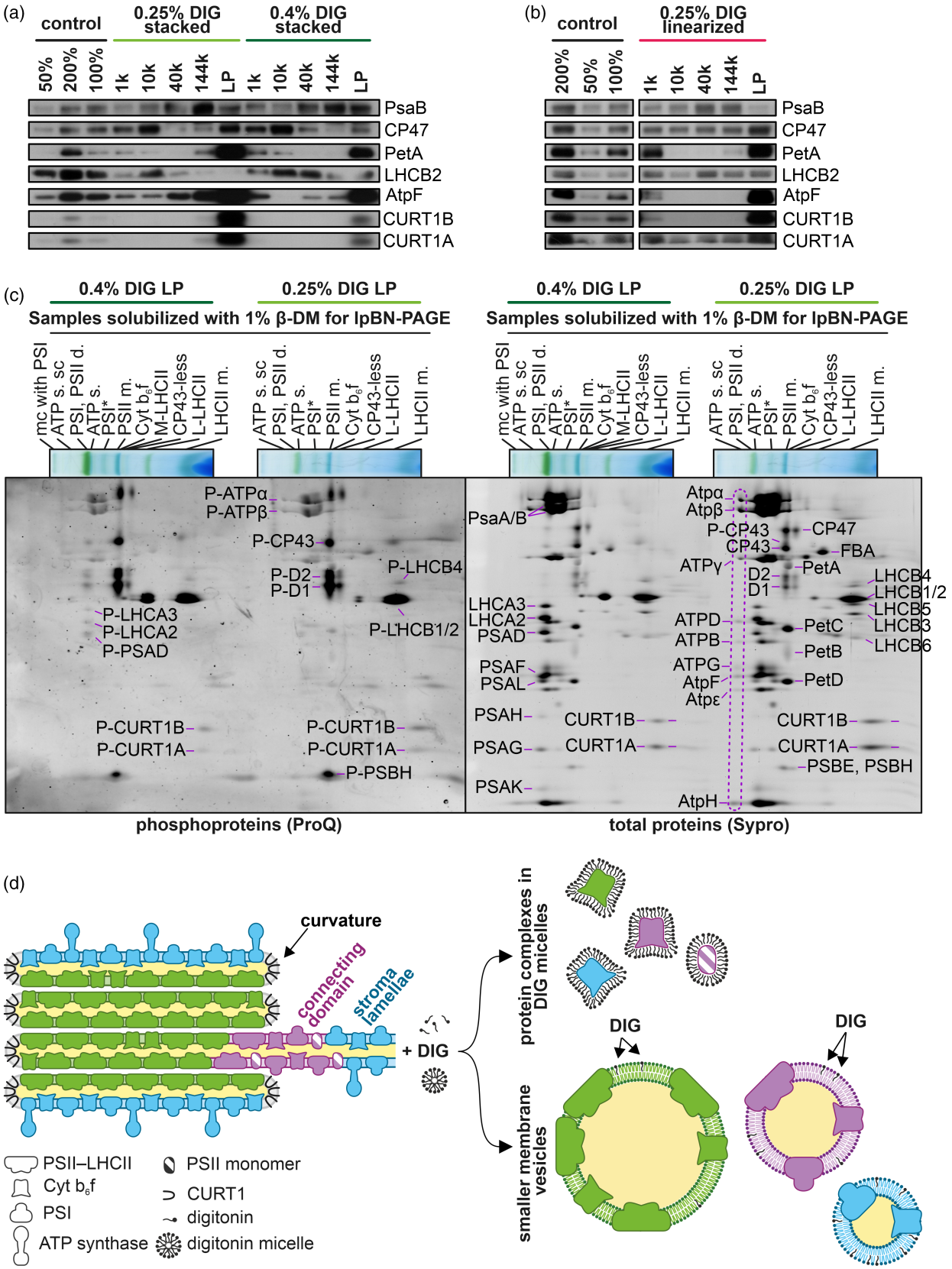

Figure 4. Effect of different [DIG] on protein accumulation in LP.
(a) Immunoblot analysis of the distribution of the major TM protein complexes (PsaB for PSI, CP47 for PSII, PetA for Cyt b_6f, LHCB2 for LHCII, AtpF for ATP synthase and CURT1B and CURT1A for CURT1) in different TM domains obtained by ultracentrifugation at the indicated speeds after solubilization of stacked TM with 0.25% (left) or 0.4% (right) DIG. Lowering [DIG] from 0.4% to 0.25% resulted in accumulation of CP47, PetA, AtpF and CURT1 proteins in LP, and concomitant decrease of PsaB and LHCB2. Samples were loaded on chl basis, each corresponding to 0.5 μg of chl. Antibody reactivity scale using 50, 100 and 200% of an intact TM sample is provided on the left.
(b) Immunoblot analysis of the distribution of the same proteins as in A upon solubilization of linearized TM with 0.25% DIG, followed by ultracentrifugation at the indicated speeds. PetA, AtpF and CURT1 proteins accumulate in LP, whereas the other protein complexes show nearly even distribution in the 10k, 40k and 144k fractions. Samples were loaded as in (a).
(c) Analysis by 2D-lpBN/SDS-PAGE of the subunit composition of the TM protein complexes accumulated in the LP fractions obtained by TM solubilization with 0.4% and 0.25% DIG. Samples corresponding to 5 μg of chl were loaded on lpBN-PAGE. Protein spots separated in the second dimension were stained first with Pro-Q Diamond (gel on the left) for phosphoprotein detection, and subsequently with Sypro to detect all proteins (gel on the right). The names of ATP synthase, PSI, PSII, Cyt b_6f and LHCII subunits are indicated according to previous publications (Aro et al., 2005; Gerotto et al., 2019; Grebe et al., 2019; Suorsa et al., 2015) A protein supercomplex (ATP s. sc) corresponding to an ATP synthase dimer (Daum et al., 2010) is highlighted by a purple dash oval.
(d) Schematic representation of the mode of action of DIG on TM. In the absence of cholesterol in the lipid bilayer, such as the TM, DIG partitions into the outer leaflet bringing to cracking the membrane in smaller vesicles of different sizes, originating from the different TM domains. Some protein complexes, such as PSII monomer and Cyt b_6f, are solubilized instead by DIG micelles. See text for details.

synthase were already solubilized by the micelles at 0.4% DIG and resolved in clearly visible bands. In contrast, PSII-LHCII sc, PSI sc and LHCII were only visible at 1% DIG. This result is consistent with the fact that proteins from different TM domains are more prone to be solubilized even by [DIG] as low as 0.25% (Figure S5c) (Trotta et al., 2019).

To further investigate the solubilization of TM protein complexes by DIG, both stacked and linearized thylakoids were solubilized lowering [DIG] to 0.1%, which has been shown to still separate the appressed and non-appressed domains (Benz et al., 2009), and the fractions were collected as in Figure 1(b). The chl *a*/*b* ratio of the fractions obtained from the stacked thylakoids showed the typical increase from 10k to 144k observed at [DIG] ≥0.25% (Figure 5b; Trotta et al., 2019). Accordingly, from the stacked TM, the PSII and LHCII accumulated in the 10k fraction and PSI in the 40k and 144k fractions (Figure 5c). On the contrary, while ATP synthase was enriched in the 40k and 144k fractions, the Cyt b_6f was almost equally present in all fractions (Figure 5c), in agreement with the results obtained by mechanical fractionation of spinach TM (Tikkanen et al., 2008). Similar behavior of Cyt b_6f and ATP synthase was also observed in linearized thylakoids solubilized with 0.1% DIG (Figure 5c). Importantly, the CURT1 proteins, although still predominantly present in the LP, were partially distributed along all fractions (Figure 5c). Analysis by lpBN-PAGE (Figure 5d; Figure S5d) showed that the PSII monomer, either from the stacked or from the linearized TM, no longer accumulated mainly in the LP but, together with CP43-less, was equally present in all fractions from the linearized TM (compare Figure 5d with Figure 2b,c). Thus, when the interaction of DIG with TM was limited by low DIG concentration, the solubilization and segregation of the Cyt b_6f, ATP synthase and PSII subcomplexes changed significantly. This suggests that at least these three protein complexes interact differently with DIG than other protein complexes such as PSII-LHCII and PSI.

Residual DIG in LP fraction modulates the properties of protein complexes

To investigate whether the presence of residual DIG and/or thylakoid lipids modulates the properties or distribution of thylakoid proteins and protein complexes in the LP fraction, we re-examined the 144k strong pellet (i.e., the SL fraction) and the co-isolated LP. Samples were homogenized to 0.25 mg chl/ml in the presence or absence of β-DM (as in Figure 2d) and loaded on BN-PAGE (Figures S6a and S7). As expected, the strong 144k pellet without β-DM did not even enter the stacking part of the BN gel, whereas the LP sample mostly entered the gel and was separated into several protein complexes (Figures S6a, right gel, and S7). Analysis by 2D BN/SDS-PAGE of the LP fraction with and without β-DM revealed that, in addition to the high MW band composed of PSI, PSII, LHCII and ATP synthase, two other protein complex bands were clearly resolved: PSII monomer and Cyt b_6f (Figure S6a,b), and to some extent also ATP synthase (Figure S7b). On the contrary, no protein complexes could be seen from the strong 144k pellet without solubilization by β-DM (Figures S6a and S7a). A likely explanation is that the protein complex bands in LP (Figure S6a,b) represent the smallest vesicles observed by TEM in LP (Figure 3), which might contain residual DIG. To test this hypothesis, the LP sample was re-centrifuged at 178 000 ***g*** (178k), to form a strong pellet, and loaded onto a lpBN-PAGE without prior solubilization with β-DM (Figures S6c and S7b). As a control, the original LP was loaded alongside, either solubilized (first lane) or not (second lane) with β-DM (Figures S6c and S7). Indeed, when the LP became a strong pellet, it could no longer enter the BN-gel (Figure S6c), and no traces of Cyt b_6f and PSII monomer could be found in 2D-lpBN/SDS-PAGE (Figure S7b). Furthermore, pelleting of LP at 178k resulted in a shift of the 77 K fluorescence emission peak from 680 (corresponding to free LHCII) to 685 nm (corresponding to PSII CP43) (Figure S6d), indicating that the presence of residual DIG interfered with the LHCII trimer structure

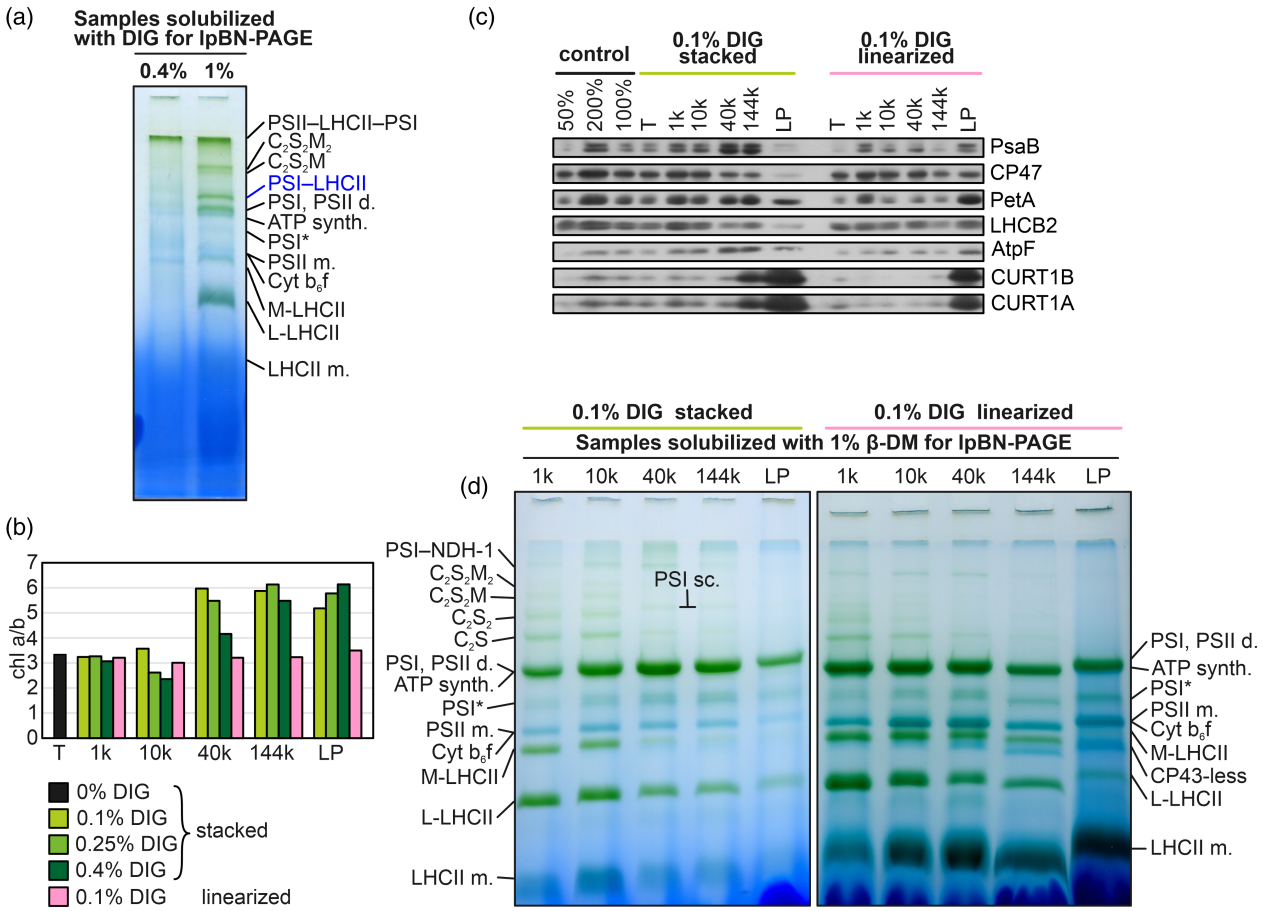

Figure 5. Limiting [DIG] differentially solubilizes the TM protein complexes.
(a) Pattern of the TM protein complexes separated by lpBN-PAGE (5 μg of chl per lane) after solubilization with 0.4% (left lane) or 1% (right lane) DIG. The major protein complexes are indicated next to the gel.
(b) Comparison of the chl *a*/*b* ratios in the 1k, 10k, 40k, 144k fractions and the LP collected at 144k after solubilization of stacked TM with 0.1% (light green), 0.25% (green) and 0.4% DIG (dark green) and linearized TM with 0.1% DIG (light pink).
(c) Immunoblot analysis of the distribution of the same proteins as in Figure 4(a,b) in different TM domains obtained by ultracentrifugation at the indicated speeds after solubilization of stacked TM (left) and linearized TM (right) with 0.1% DIG. Cyt b_6f (PetA) is almost equally distributed in all fractions, whereas the CURT1 proteins are still mostly accumulated in the LP collected at 144k. Samples were loaded on chl basis (0.5 μg of chl per lane). Antibody reactivity scale using 50, 100 and 200% of an intact TM sample is provided on the left.
(d) Analysis by lpBN-PAGE of the protein complexes accumulated, after solubilization of stacked (left) and linearized (right) thylakoids with 0.1% DIG, into the fractions obtained by differential centrifugation at 1k ***g***, 10k, 40k, 144k and the LP at 144k. Each fraction was solubilized with 1% β-DM and 5 μg of chl loaded per lane. The major protein complexes are indicated next to the gels. A PSI supercomplex (PSI sc), corresponding to a PSI dimeric complex is indicated as in Figure 2.

and/or association with PSII, as was recently described (Graça et al., 2021). Thus, pelleting removed the disruptive effect of DIG, but did not induce aggregation of the protein complexes, which indeed separated in a pattern similar to that of the original LP upon solubilization with 1% DIG prior loading (Figure S7c). This latter result provided evidence that the PSII monomer and Cyt b_6f segregate into LP due to a different interaction with the DIG micelles compared to other protein complexes. This effect was strongly attenuated by lowering [DIG] to 0.1%, as seen by running the corresponding LP in lpBN-PAGE without prior solubilization with 1% DIG (Figure S5d) where the PSII and Cyt b_6f bands are not visible.

To test whether PSII monomer and Cyt b6f segregate into lighter vesicles (LP) at any centrifugation speed, we collected the LP already formed at the 40k centrifugation step (CD LP) (Figure 1b; Figure S1), as well as the strong pellet and LP formed at the next 144k step (named as S′ and LP′, respectively) and compared them with the standard 144k and LP fractions (144k and LP) (Figure S8a). Similar to the control LP collected at 144k, both PSII monomer and Cyt b_6f were clearly enriched in the CD LP fraction (Figure S8b), indicating that they are excised by DIG from TM vesicles and accumulated as the lightest fraction (the LP) at any speed. In addition, two spots of CURT1A and CURT1B were clearly visible in the CD LP (Figure S8b).

Interestingly, the 77 K fluorescence spectrum of CD LP showed the detached LHCII peak around 680 nm similar to that in LP and LP′ (Figure S8c), confirming that this peak is due to interference from residual DIG in the sample (see Figure S6d).

Proteome composition of thylakoid subfractions after 0.25% DIG solubilization

The biochemical characterization of the LP fraction showed a different tendency of thylakoid protein complexes and/or domains to be solubilized by 0.25% DIG (Figures 2 and 3). Based on the results presented so far, it could be assumed that the fractions obtained at 10k, 40k and 144k ***g*** represented from heavier to lighter membrane vesicles derived from stacked and stroma-exposed TMs (Figure 4d). To determine how much they are enriched in the functional domains (grana core, CD, SL and curvature), the relative abundances of the proteins from the three fractions, together with LP and the intact thylakoids, were evaluated by quantitative proteomics (Figure 6). A total of 1122 proteins identified with at least two peptides were found in all fractions, of which 821 were plastidial or possibly plastidial (see legend in Data S1), while 301 were contaminants from other cellular compartments (Figure 6a; Data S1). Approximately 86% of the plastidial accessions were partially or fully characterized proteins that could be categorized by their association with protein complexes, metabolic pathways or functional categories (see legend in Data S1 for detailed description). The localization of the majority (69%) of the plastidial proteins was in the TM (membrane spanning or associated with membrane protein complexes), while smaller fractions could be localized in the chloroplast envelope (11%), thylakoid lumen (7%), plastoglobuli (4%) and the remaining (9%) were stromal proteins associated with carbon and amino acid metabolism (Figure 6a, pie chart 1).

Subsequent quantification of the relative abundance of the proteins, with respect to the intact thylakoids, revealed a strong enrichment of the majority of identified plastidial proteins in the LP (Figure 6b). This was not surprising considering that: (i) the TM fractions were quantified on the basis of chl and (ii) the procedure (reduction of [DIG] to 0.25%), which led to the accumulation of CURT1 as a kind of signature of 'purified' curvature in the LP, resulted in a very low yield of chl-binding proteins in the LP (Figure 4; Trotta et al., 2019). Therefore, by digesting the proteins based on the same [chl] in all samples, it is highly conceivable that the non-chl-binding proteins were overrepresented in the CURT1-containing LP fraction (Figure 6b). However, a relative quantification of the protein amounts in the thylakoid fractions based on the protein content, which includes non-plastidial contaminants, would also have biased the results, but in the opposite direction. To dissect the content of the CURT1-containing fraction (curvature domain), the identified plastidial proteins were further sorted into functional categories related to chloroplast metabolic, biosynthetic and repair processes (Figure 6a, pie charts 2 and 3; Data S1).

A large number of proteins/complexes (Figures 6b and 7; Figure S9; Data S1) showed the highest enrichment in the grana core fraction – 10k (e.g., PSII core, LHCII complexes, PSBS and STN8; for the full name of the proteins mentioned hereafter refer to Data S1). The SEM collected as a CD fraction (40k) showed on average the highest enrichment in PSI, LHCI belt, NDH-1 complex and FTSH protease complexes. Interestingly the thylakoid formation 1 (THF1) protein co-localized at 40k with a similar relative abundance to the FTSH protease complex (Figures 6b and 7; Figure S9; Table 1). The SPPA peptidase, which may have overlapping functions with Clp and FTSH (Nishimura et al., 2017), was also mostly enriched in the 40k and 144k fractions (Table 1). Proteins from another functional category – the chloroplast translation machinery (ribosomes and associated proteins) – showed the highest enrichment in either the 40k or 144k fraction, but a clear depletion in the LP, with some exceptions such as RPL16, a component of the chloroplast ribosomal large subunit, which segregated in the LP (Data S1). In addition to ribosomes, the SEM collected as the SL fraction (144k) also showed the highest average enrichment of pyruvate dehydrogenase complex (PDC) and VESICLE-INDUCING PROTEIN IN PLASTIDS 1 (VIPP1), involved in membrane remodeling (Gupta et al., 2021; Zhang et al., 2012).

The LP fraction, which accumulated the CURT1 proteins as a fingerprint (Figures 6b and 7; Figure S9), was also highly enriched in Cyt b_6f and ATP synthase complexes, in line with the immunoblot results (Figures 4 and 5), as well as the STN7 kinase, while the counteracting phosphatase TAP38 (Rochaix et al., 2012) was enriched in the 40k and 144k. LP also contained most of the proteins related to thylakoid architecture, such as RIQ2, the photoprotection-related protein SOQ1 and the chloroplast lipocalin (CHL), as well as most of the proteins involved in tetrapyrrole metabolism or associated with plastoglobuli (Figures 6b and 7; Figure S9; Table 1; Data S1). More specifically, the proteins of the tetrapyrrole biosynthetic pathway that are physically associated with the TM (Wang & Grimm, 2021) were indeed found to be enriched in the LP, whereas the other proteins that do not directly interact with the TM were essentially lost during fractionation (Data S1), with notable exceptions. CHLG, which converts chlorophyllide (chlide) to chlorophyll and contains a transmembrane domain (TMD), was enriched in both 144k and LP. CAO, which converts both chlide and chl *a* to chl *b* (Wang & Grimm, 2021), was enriched in 10k and LP. The transmembrane spanning FLU was equally enriched in all SEM fractions, whereas its interactors CHL27, Glu-TR and POR were only enriched in LP.

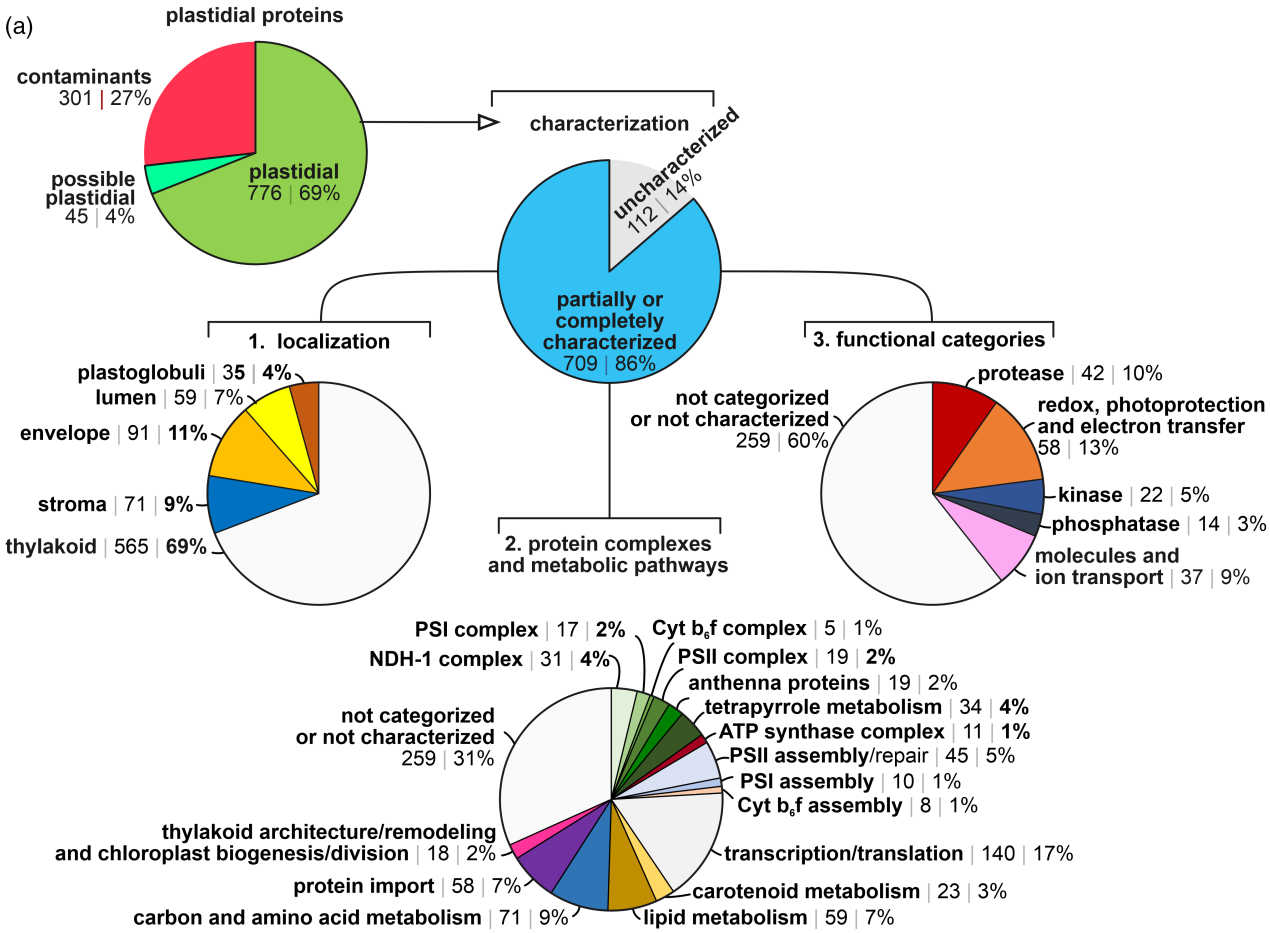

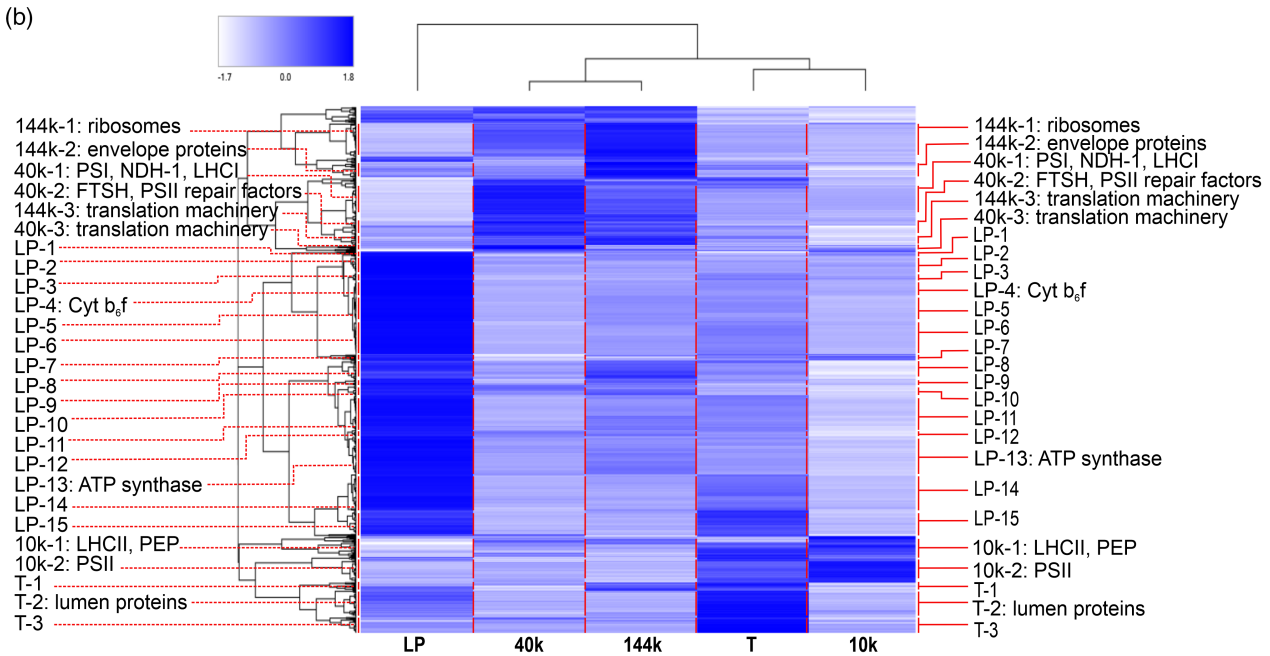

Figure 6. Identification by mass spectrometry and sorting of plastidial proteins.
(a) Pie charts depicting sorting of the 1123 proteins identified by at least two peptides. Upper pie chart, on the left: sorting according to subcellular localization. Lower pie charts: sorting according to characterization. The 821 plastidial proteins were sorted by three types of categories (lower three pie charts): (1) localization in the plastid; (2) association with protein complexes and/or metabolic pathways and (3) functional categories. The details of the sorting in categories indicated in the pie charts are presented in the legend tab in Data S1.
(b) Heat map of the relative protein abundances in the fractions obtained by DIG solubilization and differential ultracentrifugation, showing that the majority of proteins are enriched in the LP fraction. The dendrogram on the top indicates the clustering of the fractions (40k and 144k on one hand, then 10k and intact thylakoids on the other hand, and the LP which is the least similar), while the dendrogram on the left indicates the clustering of proteins with similar abundances across the fractions. The major clusters are highlighted by vertical red traits aside of each column and named according to the fraction where their relative abundance is the highest. Some of the major protein categories are indicated. A magnification of each cluster, showing the ID of the individual proteins, is presented in Figure S9.

A number of auxiliary proteins involved in PSII assembly/repair processes at different levels (Järvi et al., 2015; Lu, 2016; Nickelsen & Rengstl, 2013) were highly enriched in the LP. These include the DEGP proteases, which are involved in D1 degradation, and the chaperones HCF244 and OHP1/2, which are associated with pre-D1 co-translational insertion into the TM (Figures 6b and 7; Figure S9). On the other hand, several other proteins, which are involved in assisting PSII repair and/or insertion of PSII subunits into the TM (such as HHL1, MPH2, HCF107, HCF173, PAM68, TRXM-4, PDF1B, ALB3, TERC and PSBN) were enriched or partially enriched (such as LPA1 and cpSRP54) in the 40k and 144k fractions (Figure 6b; Figure S9; Table 1; Data S1). Curiously, although the insertase ALB3 interacts with the cpSEC1 TM translocase machinery, the components of the latter, that is, SCY1 and SECA1/AGY1 were mainly enriched in LP, as was SECE1, which was also partially enriched in 40k. The components of the cpTAT pathway HCF106, TATA and TATC/APG2, which are involved in the translocation of folded proteins, were all enriched in LP.

Among the proteins involved in PSII assembly/repair and other processes, several are lumenal proteins that were not enriched in any fraction or were rather lost during fractionation (CTPA, FKBP20-2, PLASTOCYANIN 1 and 2, PSBP and PSBQ, CYP38, HCF136 and DEGP8). Others, however, were found instead at 10k (PSBO) or 40k (TL20.3), while many soluble proteins naturally present in the thylakoid lumen or loosely associated with the TM on the stromal or lumenal side, were often segregated with LP (DEGP1, DEGP5, VDE, ZEP, CHL and PPL1) (Figure 6b; Figure S9; Table 1; Data S1).

The 10k fraction also contained several proteins associated with the membrane-bound transcriptionally active chromosome (TAC) (Figure 7; Figure S9; Table 1; Data S1). These included most of the subunits of the plastid-encoded RNA polymerase (PEP) (Figure 7), the PLASTID TAC (PTAC) proteins (-3, -5, -6, -10, -11/WHIRLY3, -12, -14 and -16), the PEP-interacting protein MurE (Garcia et al., 2007) and a partial enrichment of associated proteins such as FLN1, FLN2, TRX-Z and FSD2 (Wu et al., 2024) (Figure 7). Interestingly, the protein pTAC5, as well as SULFITE REDUCTASE (SIR), which, in addition to its enzymatic activity, also binds nucleoids and interacts with PTAC10 (Jeon et al., 2012), both showed a strong enrichment at 40k (Table 1). Another protein with moonlighting activity like SIR, that is, the E2 subunit of the pyruvate dehydrogenase complex (PDC) which binds *psbA* mRNA (Watkins et al., 2020), was instead enriched in the 144k fraction. A further set of mRNA-binding proteins, the pentatricopeptide repeat (PPR) proteins, which are involved in mRNA processing with high specificity (Meng et al., 2024), were found to be associated with the TM (Figure 6b; Figure S9; Data S1). These include AT5G13770, SVR7 (involved in ATP synthase accumulation), MRL1 (involved in Rubisco accumulation), PPR4 and CRP1 (involved in Cyt b_6f subunit accumulation), and the psbA mRNA binding protein HCF173, all of which were enriched in the 40k and 144k fractions. Further two RNA binding proteins, that is, CSP41B (which, like HCF173, is a member of the short dehydrogenase-reductase (SDR) family) and SOT1, which is involved in rRNA processing, were instead mostly present in the 10k fraction (Figure 6b; Figure S9; Table 1; Data S1).

DISCUSSION

Advances in bioimaging technologies used to study TM architecture have revealed a higher complexity than previously expected in the composition, distribution and dynamics of the photosynthetic machinery (Bussi et al., 2019; Daum & Kuhlbrandt, 2011). Such complexity requires dedicated biochemical approaches to investigate the 3D heterogeneity of the TM (Figure 1a), both structurally and functionally. Mechanical fractionation of the TM would probably be the most optimal approach for this purpose but has not yet been successful in the model plant Arabidopsis. The main thylakoid domains, that is, the appressed grana membranes (10k fraction) and the non-appressed SL (144k fraction), have been extensively studied (Andersson & Anderson, 1980; Danielsson & Albertsson, 2009; Tomizioli et al., 2014). Conversely, the composition, location and function of the enigmatic thylakoid domain known as the grana margin (GM) has remained controversial (Anderson, 2012; Koochak et al., 2019; Puthiyaveetil et al., 2014; Rantala et al., 2020; Tomizioli et al., 2014; Trotta et al., 2019), despite the critical

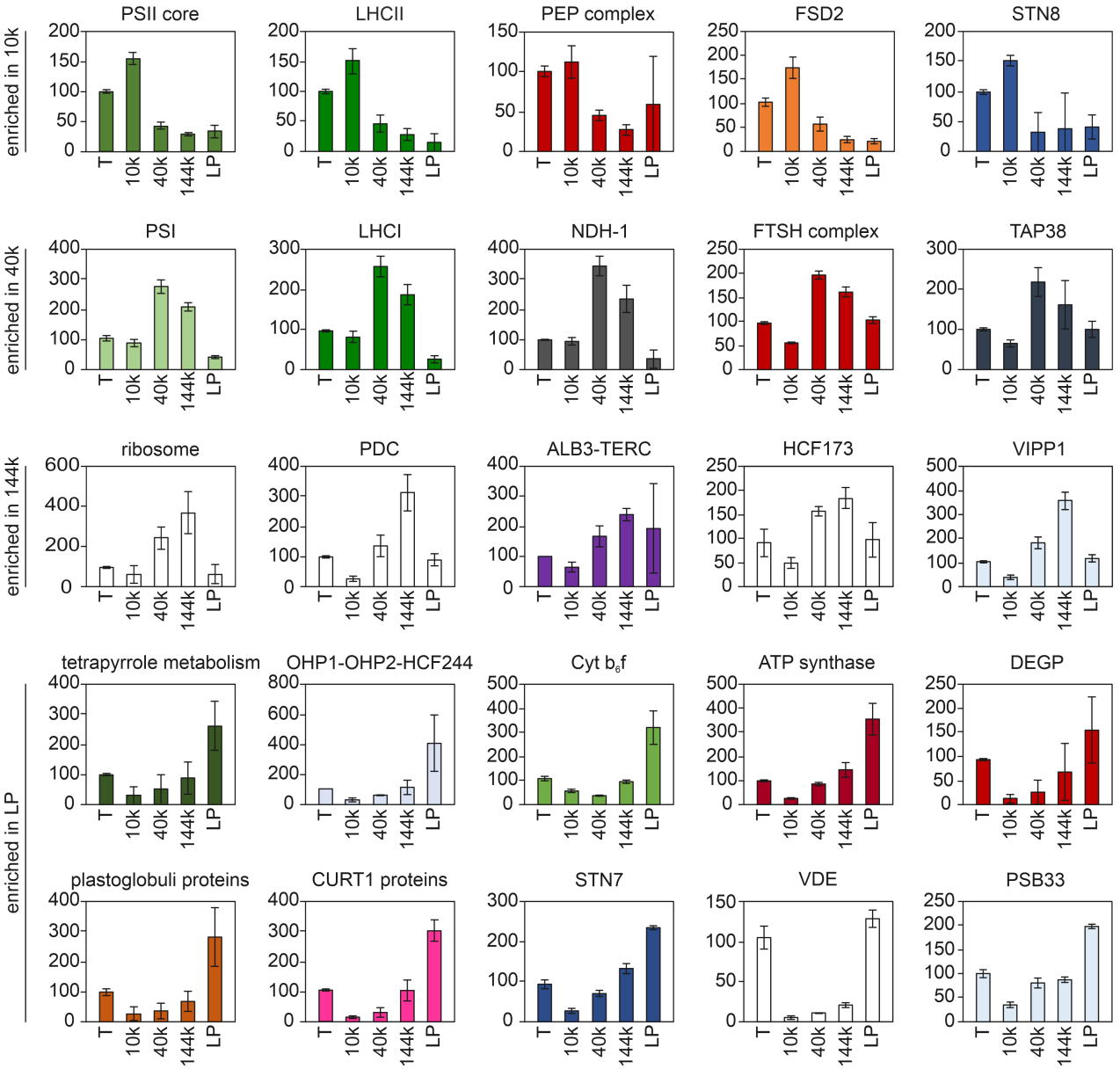

Figure 7. Enrichment of proteins and protein complexes in TM fractions.
The boxes show the relative accumulation (as in Data S1) of the protein subunits of the major TM protein complexes, proteins specific to biosynthetic pathways or TM structures, and specific proteins involved in processes like post-translational modifications, degradation, or co-translational insertion into the TM, in the different TM fractions collected at 10k, 40k, 144k or LP collected at 144k, compared to intact TM (set as 100%), after solubilization with 0.25% DIG. Proteins or protein complexes which show enrichment, on average, in one or another fraction were separated in the corresponding groups labeled on the left. Bars represent SD (n = 3). The locus identifiers and gene symbols used for quantification of the proteins and protein subunits of the protein complexes are indicated in Data S2.

importance of the GM for thylakoid dynamics, especially under fluctuating light conditions. Here we propose that the GM is composed of two separate TM domains, which we define as the connecting domain (CD, 40k fraction) and the curvature domain (present in the LP fraction with CURT1 proteins as fingerprints) (Figure 1a). This proposal is based on a thorough reconsideration of the biochemical isolation and the functional roles of the curvature and CD in the light-driven photosynthetic process of the TM.

Three key messages from TM biochemical fractionation

First, by comparing the protein complexes pattern in stacked and linearized thylakoids, we investigated whether and why the TM folding into appressed (stacked) and

Table 1 List of selected proteins involved in PSII assembly or repair cycle or other relevant pathways enriched in either the 40k, 144k or the LP fraction

Gene name	Trans membrane-domain (TMD)	Locus identifier	Relative abundance vs thylakoid (=100)			
			10K	40K	144K	LP
Lipocalins and related proteins						
ZEAXANTHIN EPOXIDASE (ZEP) (ABA1)		AT5G67030	13 ± 1	31 ± 1	62 ± 10	304 ± 18
CHLOROPLASTIC LIPOCALIN (CHL)		AT3G47860	12 ± 1	19 ± 2	53 ± 14	308 ± 18
TEMPERATURE-INDUCED LIPOCALIN (TIL)		AT5G58070	24 ± 5	30 ± 2	70 ± 13	343 ± 29
SUPPRESSOR OF QUENCHING 1 (SOQ1)	TMD	AT1G56500	36 ± 5	104 ± 2	118 ± 6	270 ± 13
RELAXATION OF QH (ROQH)		AT4G31530	13 ± 2	15 ± 6	25 ± 13	214 ± 6
Proteases and related proteins						
PSB29/THF1	TMD	AT2G20890	57 ± 9	195 ± 18	179 ± 18	111 ± 4
FTSH5 INTERACTING PROTEIN (FIP)	TMD	AT5G02160	97 ± 19	109 ± 5	96 ± 13	48 ± 9
FTSH PROTEASE 6 (FTSH6)	TMD	AT5G15250	356 ± 272	183 ± 70	124 ± 86	105 ± 94
FTSH PROTEASE 11 (FTSH11)	TMD	AT5G53170	81 ± 15	163 ± 11	129 ± 33	224 ± 17
SIGNAL PEPTIDE PEPTIDASE (SPPA)		AT1G73990	55 ± 1	223 ± 7	229 ± 26	110 ± 3
Transcriptionally active chromosome (TAC) proteins						
SULFITE REDUCTASE (SIR)		AT5G04590	89 ± 15	346 ± 47	202 ± 13	29 ± 2
STF		AT3G48500	121 ± 23	49 ± 9	45 ± 15	28 ± 9
PLASTID TRANSCRIPTIONALLY ACTIVE 5 (PTAC5)		AT4G13670	188 ± 34	356 ± 6	142 ± 13	50 ± 9
MurE		AT1G63680	145 ± 26	76 ± 39	56 ± 28	25 ± 5
Transcription and translation						
HIGH-CHLOROPHYLL-FLUORESCENCE 101 (HCF101)		AT3G24430	44 ± 11	380 ± 65	47 ± 11	100 ± 22
FERRITIN 4 (FER4)		AT2G40300	11 ± 1	95 ± 20	266 ± 84	162 ± 38
CHLOROPLAST RNA PROCESSING 1 (CRP1)		AT5G42310	58 ± 9	148 ± 12	139 ± 60	84 ± 29
CP33A/RBP31		AT4G24770	73 ± 10	213 ± 67	189 ± 101	28 ± 17
MATURATION OF RBCL 1 (MRL1)		AT4G34830	60 ± 3	211 ± 24	192 ± 49	98 ± 20
MORF2		AT2G33430	2349 ± 569	2065 ± 839	17338 ± 314	402 ± 211
MORF9		AT1G11430	243 ± 36	477 ± 105	80 ± 34	217 ± 17
WHAT IS THIS FACTOR 1 (WTF1)		AT4G01037	65 ± 12	214 ± 74	106 ± 27	25 ± 4
CRS1/YhbY (CRM) domain-containing protein	TMD	AT3G18390	69 ± 67	154 ± 72	94 ± 26	73 ± 32
HIGH CHLOROPHYLL FLUORESCENT 107 (HCF107)		AT3G17040	62 ± 11	223 ± 50	238 ± 60	114 ± 35
SUPPRESSOR OF VARIEGATION 7 (SVR7)		AT4G16390	37 ± 10	126 ± 28	99 ± 33	100 ± 25
CP33B		AT2G35410	45 ± 14	148 ± 14	180 ± 25	87 ± 33
CP33C		AT4G09040	68 ± 12	176 ± 15	212 ± 35	86 ± 35
PSII assembly factors during repair cycle: D1 damage and degradation						
HYPERSENSITIVE TO HIGH LIGHT 1 (HHL1)	TMD	AT1G67700	77 ± 8	233 ± 35	267 ± 78	63 ± 10
LOW QUANTUM YIELD OF PHOTOSYSTEM II 1 (LQY1)	TMD	AT1G75690	13 ± 1	30 ± 5	47 ± 14	88 ± 2
PSB27		AT1G03600	85 ± 10	95 ± 8	73 ± 8	102 ± 9
CYCLOPHILIN 38 (CYP38)		AT3G01480	24 ± 3	28 ± 2	22 ± 2	51 ± 7
PHOTOSYSTEM II REACTION CENTER PSB28		AT4G28660	33 ± 10	73 ± 5	104 ± 27	374 ± 53
PHOTOSYNTHESIS AFFECTED MUTANT 68 (PAM68)	TMD	AT4G19100	59 ± 19	146 ± 14	133 ± 18	99 ± 39
HCF173		AT1G16720	55 ± 11	159 ± 10	188 ± 22	93 ± 36
PEPTIDE DEFORMYLASE 1B (PDF1B)		AT5G14660	45 ± 4	153 ± 7	132 ± 54	33 ± 10
CHLG	TMD	AT3G51820	43 ± 4	120 ± 12	210 ± 30	224 ± 4
PSBN	TMD	ATCG00700	53 ± 13	113 ± 5	144 ± 20	84 ± 25
LOW PSII ACCUMULATION1 (LPA1)	TMD	AT1G02910	46 ± 7	132 ± 15	153 ± 7	209 ± 3
PSII assembly factors during repair cycle: After insertion of newly synthesized D1						
MPH2		AT4G02530	27 ± 5	90 ± 2	57 ± 3	95 ± 2
PSBP-LIKE PROTEIN 1 (PPL1)		AT3G55330	14 ± 2	26 ± 3	37 ± 1	102 ± 10
HIGH CHLOROPHYLL FLUORESCENCE 136 (HCF136)		AT5G23120	12 ± 2	30 ± 2	33 ± 2	93 ± 4
MET1		AT1G55480	10 ± 1	19 ± 2	44 ± 8	212 ± 27
MPH1	TMD	AT5G07020	35 ± 7	76 ± 3	63 ± 4	144 ± 7

(continued)

Table 1. (continued)

Gene name	Trans membrane-domain (TMD)	Locus identifier	Relative abundance vs thylakoid (=100)			
			10K	40K	144K	LP
PHOTOSYSTEM B PROTEIN 33 (PSB33)		AT1G71500	34 ± 6	75 ± 10	84 ± 6	196 ± 5
THYLAKOID LUMEN PROTEIN 18.3 (TLP18.3)	TMD	AT1G54780	136 ± 9	73 ± 5	66 ± 4	63 ± 4
FKBP20-2		AT3G60370	7 ± 2	7 ± 1	9 ± 5	57 ± 1
ROTAMASE CYP 4 (ROC4); CYP20-3		AT3G62030	13 ± 4	11 ± 2	13 ± 1	46 ± 7
RBD1	TMD	AT1G54500	37 ± 4	105 ± 8	111 ± 7	194 ± 14
LIGHT-HARVESTING-LIKE 3:1 (LIL3:1)	TMD	AT4G17600	27 ± 6	67 ± 2	115 ± 10	227 ± 36
LIGHT-HARVESTING-LIKE 3:2 (LIL3:2)	TMD	AT5G47110	16 ± 4	41 ± 4	93 ± 16	259 ± 18
THIOREDOXIN M-TYPE 1 (THM1)		AT1G03680	15 ± 3	33 ± 1	57 ± 1	224 ± 14
THIOREDOXIN M-TYPE 4 (TRX-M4)		AT3G15360	29 ± 3	79 ± 8	39 ± 5	63 ± 5
THIOREDOXIN M-TYPE 2 (ATHM2)		AT4G03520	14 ± 4	29 ± 1	73 ± 3	244 ± 7
PSII subunits						
PHOTOSYSTEM II SUBUNIT S (PSBS)	TMD	AT1G44575	150 ± 4	29 ± 4	34 ± 6	37 ± 3
PHOTOSYSTEM II SUBUNIT O-2 (PSBO2)		AT3G50820	123 ± 6	21 ± 1	11 ± 1	18 ± 3
PS II OXYGEN-EVOLVING COMPLEX 1 (PSBO1)		AT5G66570	129 ± 6	20 ± 3	9 ± 1	14 ± 2
cpTAT pathway						
HIGH CHLOROPHYLL FLUORESCENCE 106 (HCF106)	TMD	AT5G52440	20 ± 2	59 ± 5	112 ± 8	338 ± 25
TWIN-ARGININE TRANSLOCATION A (TATA)	TMD	AT5G28750	14 ± 5	42 ± 5	130 ± 26	236 ± 56
ALBINO AND PALE GREEN 2 (APG2) (TATC)	TMD	AT2G01110	8 ± 1	71 ± 16	149 ± 27	374 ± 35
cpSEC pathway						
SECE1	TMD	AT4G14870	45 ± 1	241 ± 22	169 ± 9	397 ± 19
SECY HOMOLOG 1 (SCY1)	TMD	AT2G18710	38 ± 4	109 ± 11	137 ± 16	288 ± 21
ALBINO OR GLASSY YELLOW 1 (AGY1) (SECA1)		AT4G01800	26 ± 2	86 ± 14	103 ± 18	183 ± 9
cpSRP pathway						
CHLOROPLAST SIGNAL RECOGNITION PARTICLE 54 KDA SUBUNIT (CPSRP54)		AT5G03940	69 ± 4	76 ± 3	93 ± 18	113 ± 14
CHAOS (CAO) (cpSRP43)		AT2G47450	35 ± 5	55 ± 6	122 ± 24	199 ± 13
cpFTSY		AT2G45770	24 ± 2	24 ± 2	24 ± 8	29 ± 10
Other lumen proteins						
CTPA		AT4G17740	11 ± 1	13 ± 0	13 ± 4	61 ± 9
Pentapeptide repeat-containing protein TL20.3		AT1G12250	92 ± 10	139 ± 7	115 ± 13	122 ± 9
PLASTOCYANIN 1 (PETE1) (1 peptide)		AT1G76100	2 ± 2	2 ± 1	2 ± 1	3 ± 2
PLASTOCYANIN 2 (PETE2)		AT1G20340	8 ± 2	21 ± 6	13 ± 5	14 ± 4
FERREDOXIN C 2 (FdC2)		AT1G32550	9 ± 4	7 ± 3	9 ± 1	182 ± 14
FZO-LIKE (FZL)		AT1G03160	14 ± 2	38 ± 4	80 ± 14	301 ± 34
Others						
TRANSKETOLASE 2 (TKL2)		AT2G45290	92 ± 90	945 ± 131	788 ± 636	131 ± 49
PGR5		AT2G05620	54 ± 5	119 ± 15	195 ± 38	270 ± 12
PGR5-LIKE A	TMD	AT4G22890	33 ± 4	70 ± 11	121 ± 15	273 ± 10
PGR5-like B	TMD	AT4G11960	24 ± 7	48 ± 6	106 ± 17	223 ± 2
THYLAKOIDAL ASCORBATE PEROXIDASE (TAPX)	TMD	AT1G77490	64 ± 4	155 ± 15	141 ± 8	95 ± 3
SOUL HEME BINDING PROTEIN 4 (SOUL4)		AT3G10130	151 ± 23	44 ± 10	36 ± 2	21 ± 5
SALT-INDUCED ABC1 KINASE 1 (SIA1)	TMD	AT3G07700	46 ± 9	197 ± 25	410 ± 31	234 ± 27
PASTOGLOBULAR PROTEIN 18 (PG18)		AT4G13200	53 ± 15	149 ± 32	298 ± 66	128 ± 13
Phosphoenolpyruvate carboxylase family protein		AT4G10750	101 ± 14	252 ± 57	231 ± 90	20 ± 4
(RIQ1)	TMD	AT5G08050	167 ± 15	23 ± 1	38 ± 10	187 ± 16
(RIQ2)	TMD	AT1G74730	72 ± 1	27 ± 2	59 ± 9	270 ± 32

Abundance is expressed as relative to thylakoids, which is set to 100, ±SD (n = 3). Proteins presented in Figure 7 are not repeated here.

non-appressed membranes affects their partitioning into different thylakoid subfractions (domains) (Figures 2–5). Fractionation of stacked TM confirmed the known heterogeneity (Dekker & Boekema, 2005; Dlouhý et al., 2021; Koochak et al., 2019) and the segregation of PSI-LHCI and PSII-LHCII towards SL and grana, respectively, while NDH-1 and significant amount of LHCII indicated that the CD was enriched in the 40k fraction (Figures 2, 4, and 7).

Conversely, such a heterogeneity was completely lost upon TM linearization, resulting in homogeneous vesicle shapes and uniform composition of protein complexes in the 10k, 40k and 144k fractions (domains) (Figures 2–4). Importantly, the LP from linearized TM was not uniform with respect to other fractions, presenting an accumulation of Cyt b_6f, PSII subcomplexes and ATP synthase similar to that obtained in LP from stacked TM, thus independently of TM folding (Figures 2 and 4).

Second, the use of DIG at different concentrations revealed the specificity of the interaction between DIG and the TM protein complexes, probably due to the influence of their distinct annular lipids on the formation of DIG micelles (Figures 3–5) (Rantala & Tikkanen, 2018; Trotta et al., 2019). Indeed, when [DIG] was reduced to a certain threshold (0.8 mM or 0.1%), the distribution of Cyt b_6f was uniform across TM domains, like it is after mechanical fractionation of TM (Danielsson & Albertsson, 2009; Tikkanen et al., 2008). This and the previous point showed that Cyt b_6f, the PSII subcomplexes and ATP synthase were particularly prone to be 'extracted' from the TM by DIG (Figure 5; Figure S6). These facts suggest that the LP cannot represent the connections between the appressed grana membranes and the non-appressed stroma lamellae, that is, the CD (Figure 1a), and indicate that the localization of CURT1 upon biochemical fractionation do not coincide with the CD.

Third, the thylakoid fractions enriched in the appressed grana, CD and SL domains, as well as in the CURT1-enriched curvature (LP) (Figure 1), were analyzed by quantitative mass spectrometry (Figures 6 and 7), providing a comprehensive picture of the distribution of more than 800 proteins. In general, most of the subunits of the major thylakoid protein complexes were clustered in the expected major TM domains. On the other hand, the protein subunits of several known holo-complexes, such as TM translocases and PSII repair/assembly intermediates, or the localization of enzymes and their protein substrates, segregated into two distinct fractions after DIG solubilization (Figure 7; Table 1; Data S1), most frequently LP and the two SEM fractions at 40k and 144k. Thus, when assessing the protein composition of the LP, it must also be considered that some of the necessary interactions between TM proteins may be disrupted despite the use of a mild detergent such as DIG.

These results point to the presence of microdomains in the TM with a specific lipid composition or even within a specific protein complex (Kobayashi et al., 2017; Theis & Schroda, 2016), which affect the DIG solubilization and subsequent separation of TM proteins and protein complexes into distinct (sub)fractions and domains, as discussed below.

DIG interaction with TM proteins is not uniform

The TM consists of approximately 70% (by molar mass) of proteins, with the remaining consisting mainly of three types of galactolipids, of which approximately 50% is monogalactosyldiacylglycerol (MGDG), 30% digalactosyldiacylglycerol (DGDG) and 5–12% sulfoquinovosyldiacylglycerol (SQDG), as well as up to 5–12% of a phospholipid, phosphatidylglycerol (PG) (Garab et al., 2022).

In cholesterol-containing membranes, DIG typically solubilizes the protein complexes along with their annular lipids (Schölz et al., 2011). However, this can apparently also occur for protein complexes from cholesterol-free membranes such as TM (Järvi et al., 2011), or inner mitochondrial membrane (IMM) (Wittig & Schägger, 2005), and indeed these protein complexes are resolved as bands in BN-PAGE (Figures 2, 4, and 5). In particular, at [DIG] >0.1% and up to 0.4%, Cyt b_6f, PSII monomer and ATP synthase are clearly visible as distinct bands in BN-PAGE (Figure 5a), whereas even higher [DIG] (i.e., ≥0.5%) is required to resolve PSI-LHCI, PSII dimer, PSII-LHCII sc and LHCII trimers in BN-PAGE (Grieco et al., 2015) (Figure 5a). Indeed, the presence of DIG between 0.1 and 0.25% is sufficient to form small vesicles (LP) containing PSII monomer and Cyt b_6f, which are resolved in BN-PAGE (Figure 3; Figure S6), but below 0.1% no separation of these complexes is observed (Figure S5d). Moreover, DIG solubilizes Cyt b_6f and PSII monomer from the TM independently of the stacking state (Figures 2 and 4), leading to their accumulation in the LP. It is also conceivable that some of the small particles observed by TEM are indeed micelles surrounding these specific lipid-depleted protein complexes (Figure 3). Why are some TM protein complexes more solubilized already at lower [DIG]? Possible explanations must take into account both the critical micellar concentration (CMC) of DIG and its interaction with specific lipids.

The lowest [DIG] for the onset of self-association in micelles is 0.013% (0.1 mM), but this process then occurs over an order of magnitude range (Fan & Heerklotz, 2017), including the 0.1% [DIG] used in this work. However, the presence of cholesterol-free lipid vesicles affects DIG self-association, resulting in simultaneous presence of DIG micelles and smaller vesicles (Fan & Heerklotz, 2017). Thus, the lack of strict linearity between increasing DIG concentration and the accumulation of a given protein complex in the LP is likely related to the dynamics of DIG micelle formation.

Saponins such as DIG are generally composed of a triterpene-derived sterol moiety (aglycone) covalently linked to one or more saccharide residues (glycone), giving rise to the amphipathic nature of saponins (Augustin et al., 2011). In the absence of cholesterol, weak interactions of saponins with phospholipids still occur, depending on the degree of hydrophilicity determined by the substitutions on both the sterol backbone and the glycone moiety (Wojciechowski et al., 2016). Among phospholipids, DIG has a preference for phosphatidylethanolamine (PE) (Orczyk et al., 2017), which, like MGDG in the TM, is a non-

bilayer lipid and also a major component of the IMM (Garab et al., 2022). Considering that the glycone moiety of DIG is essential for interaction with lipid polar heads (Nishikawa et al., 1984), it is conceivable that in sterol-free TM, DIG interacts differently with the uncharged saccharide polar heads of MGDG and DGDG compared to the negatively charged SQDG and PG. Thus, an interaction between DIG and the phospho- or galactolipids of the annular ring, which interact with the protein TMD and thus have specific biophysical properties (Pàli et al., 2003), may influence the solubilization of protein complexes such as PSII monomer and Cyt b_6f. This could be exacerbated by the fact that the TM has a high protein/lipid ratio, which limits the lipid-occupied surface available for interaction with DIG (Garab et al., 2022).

Potential role of annular lipids in extraction of protein complexes by DIG

Although the bulk glycerolipids do not show lateral heterogeneity in the TM domains (Duchêne & Siegenthaler, 2000), lipids form clusters according to the properties of their polar heads and lipid tails (van Eerden et al., 2015), and the annular lipids around and inside the protein complexes are highly heterogeneous (Kobayashi et al., 2017). Accordingly, the characteristics of the annular lipids may, at least in part, explain the controversial localization of TM protein complexes reported in the literature. For example, mechanical TM fractionation shows a rather uniform distribution of Cyt b_6f along the entire TM (Albertsson et al., 1991; Danielsson & Albertsson, 2009; Romanowska & Albertsson, 1994; Tikkanen et al., 2008), suggesting its presence also in the grana core, which provides a short pathway for PQH_2 oxidation (Cramer, 2019; Johnson et al., 2014; Tremmel et al., 2003). On the other hand, it has been shown that Cyt b_6f is particularly susceptible to being 'excised' from the membrane by both α-DM and TRITON X-100 (Johnson et al., 2014; van Roon et al., 2000). Furthermore, DIG and cholate, which share part of the steroid backbone, have been used for partial purification of Cyt b_6f (Hurt & Hauska, 1981; Nelson & Neumann, 1972; Pick & Racker, 1979). Thus, the interaction between DIG and the annular lipids with specific properties surrounding Cyt b_6f in TM (Swainsbury et al., 2018) may be the cause for the accumulation of Cyt b_6f into the LP fraction (Figure 4).

Similarly, the tendency of PSII monomer to segregate into the LP (Figures 2 and 4; Figure S8) may also be linked to the interaction of DIG with a distinct annular lipid environment in the intact TM. For instance, DIG integrates into specific hydrophobic niches in isolated PSII complexes (Graça et al., 2021), and indeed residual DIG in the LP affects BN-PAGE migration of PSII monomers and causes a shift of the 77 K fluorescence peak from 685 nm (PSII monomer) to 680 nm (LHCII) (Figure S6) (Mohamed et al., 2022). Moreover, a specific lipid environment is suggested by the fact that monomerization of PSII is associated with deacylation of specific lipids in the monomer-monomer interphase (Jimbo & Wada, 2023; Kruse et al., 2000). A further evidence that the annular lipids of PSII monomers or Cyt b_6f may be specific is that, unlike PSI-LHCII and PSII-LHCII complexes, they are not solubilized into nanodiscs by the non-detergent poly(styrene-maleic acid)s (pSMA) (Bell et al., 2015; Korotych et al., 2019, 2021; Scheidelaar et al., 2015). Interestingly, SMA interactions with galactolipids differ from those with phospholipids (Phan et al., 2020), and such a differential interaction may also be the case in the action of DIG (see above).

CURT1-associated curvature and co-isolated proteins

Based on the small size and the shape of the vesicles in the CURT1-containing fraction (LP), it is highly likely that the curvature as an intact domain represented by curved vesicles is not isolated by DIG (Figure 3). DIG is widely used to solubilize membranes with >10 mol% cholesterol (Fan & Heerklotz, 2017; Sudji et al., 2015). However, the TM does not contain cholesterol, which means that DIG is only partitioned into the outer leaflet of the membrane bilayer. This leads to asymmetric stress in the bilayer (Fan et al., 2016; Fan & Heerklotz, 2017) and eventually to the formation of TM vesicles of different sizes, as observed by TEM (Figures 3 and 4d), which remain partially stacked when originating from the grana core (Dlouhý et al., 2021; Dunahay et al., 1984). These vesicles, in the 10k, 40k and 144k fractions, are virtually free of CURT1 proteins, which are mostly removed by even the lowest [DIG] (Trotta et al., 2019; Figure S5c). Regarding the other proteins co-isolated with CURT1, the accumulation of Cyt b_6f and PSII monomer in LP is highly dependent on the [DIG] used (see above) and thus, at least in part, does not reflect the natural composition of the curvature. The same is true for ATP synthase, which is distributed in all stroma-exposed domains in intact TM (Daum et al., 2010), but is mostly enriched in the LP after fractionation.

Is there a link between the isolation of CURT1 and the TM lipid phase? CURT1 proteins contain an amphipathic alpha-helical domain typical of proteins involved in the bending biological membranes, including the highly curved stroma-exposed domains such as the peripheral curvature of grana discs and the left-handed helices of SL (Figure 1) (Bussi et al., 2019; Giménez-Andrés et al., 2018; Könnel et al., 2019). This amphipathic domain has been shown to act on the polar heads of lipids, in some cases preventing the formation of non-bilayer phases, typical of lipids such as MGDG (Thalhammer & Hincha, 2014). The non-bilayer phases, such as the hexagonal phase (H_{II}) of MGDG, may play a role in the dynamic modulation of the TM lipid composition and flexibility, both in the grana core (Seiwert et al., 2017; Simidjiev et al., 2000) and at the curvature of the grana discs (Murphy, 1982; Raven, 2021).

Other proteins associated with non-bilayer phases and found in the LP are the lipocalins such as VDE and ZEP (Dlouhý et al., 2020) (Table 1 and Figure 7). Are lipocalins then associated with the curvature domain in intact TM? This is unlikely the case, since VDE in intact thylakoids functionally interacts with LHCII-associated violaxanthin in the grana core and CD, but there is only a very minor amount of LHCII in the LP (Figures 2 and 4). Furthermore, VDE is a lumen protein. While lumen proteins can be either strongly associated with the lumen surface of the TM or free in the lumen (Gollan et al., 2021), we did not observe a strict relationship between this property and their enrichment in strong pellets (10k, 40k and 144k) or LP (Table 1; Data S1), suggesting that the fractionation procedure and/or the interaction with DIG is the main reason for their enrichment in each isolated fraction.

On the other hand, we observed a strong enrichment of plastoglobuli proteins in the LP (Figures 6 and 7; Data S1). This is consistent with the fact that plastoglobuli are associated with all types of curvature domains in SEM (Daum & Kuhlbrandt, 2011), all of which could be shaped by CURT1 proteins (Bussi et al., 2019). Indeed, this could justify the enrichment of lipids observed in the LP by (Koochak et al., 2019).

In general, several of the proteins found by mass spectrometry in the LP fraction are components of molecular machines whose counterparts are enriched at 40k and 144k (Data S1). Thus, any conclusions drawn from the protein composition of the LP fraction must take in account the structurally and biochemically proven interactions of the proteins with their functional partners, as discussed above for Cyt b_6f and PSII-LHCII.

PSI supercomplexes with LHCII and NDH-1 are specific for the CD domain

The 10k fraction (grana core) was clearly enriched in protein subunits forming the PSII core and LHCII complexes (Figure 7). However, the LHCII trimer associated with PSI (the so-called state complex) was mainly enriched in the 40k fraction and, to a lesser extent in the 144k fraction (Figure 2; Figures S2 and S8), suggesting some degree of cross-contamination between CD and SL. The presence of a relevant amount of M- and L-LHCII in the 40k fraction, clearly more than in 144k (Figures 2b,c and 4a; Figures S3a, S5b, and S8a), indicates that the 40k vesicles (Figure 3) originate from SEM closer to grana than those in 144k. These two pieces of evidence, based on proteomics and BN-PAGE analysis, together with the lower chl *a*/*b* ratio of the 40k fraction compared to 144k (Figures 2b and 5b; 0.25 and 0.4% DIG), indicate the enrichment of CD in the 40k fraction.

Also, the NDH-1 complex, together with the LHCA isoforms A5 and A6, which link NDH-1 to PSI to perform cyclic electron flow (CEF), were enriched in the CD (40k) and slightly less in the SL (144k) (Figure 7; Data S1), (Peng et al., 2009; Shen et al., 2021; Su et al., 2022). In this context, the proteins PGR5, PGRL1A and PGRL1B, putatively related to another CEF functioning around PSI in SEM, were instead enriched in the LP, which is mostly depleted of PSI. This is consistent with the fact that these PGR proteins do not form a stable complex with PSI. The proteomic analysis also revealed other cases where functionally related proteins were segregated into separate fractions by the biochemical treatment with DIG. For example, the segregation of the STN7 kinase and VDE in LP, which contrasts with the localization of their substrate LHCII (as a protein or as associated with violaxanthin, respectively), enriched at 10k (Figure 7). On the other hand, STN7 interacts with Cyt b_6f (Rochaix et al., 2012), which might explain its enrichment in LP.

Transcription/translation machinery enriches in CD (40k) and SL (144k)

The SEM fractions 40k and 144k were enriched in almost all of the 140 identified proteins involved in chloroplast transcription and translation (Figure 7; Data S1), including the pTAC-associated proteins, such as the PEP complex and its interacting partner FSD2 (Wu et al., 2024), and the ribosomal subunits and proteins involved in mRNA processing, translation initiation and elongation (Olinares et al., 2010), while only a few accumulated in the LP. The nucleoid-associated proteins were found in the 10k (Figure 7; Table 1; Data S1), in agreement with previous reports (Tomizioli et al., 2014). The presence of part of the transcriptional machinery in the 10k probably indicates that part of the CD domain is located in this fraction, most likely due to the mild solubilization with only 0.25% DIG. The translation machinery, on the other hand, was partly enriched in CD (40k) and partly in SL (144k). Many of these proteins are required for mRNA stabilization and editing (MORF2, MORF9, CP33B and CP33C). MORF2 and MORF9 were found to interact with part of the tetrapyrrole biosynthetic machinery, the majority of components of which were found in the LP in this and other studies (Maeda et al., 2022; Wang et al., 2020), suggesting that the tetrapyrrole biosynthetic pathway is in fact associated with the domains enriched in the 40k and 144k in intact TM. Several other proteins enriched at 40k, 144k or both (Table 1) are required for the co-translational processing of chloroplast-encoded subunits of the major protein complexes such as PSII (HCF173, HCF107 and PDF1B), Cyt b_6f (CRP1, HCF107 and WTF1), NDH-1 (WTF1) and ATP synthase (CRS1 and SVR7) (Table 1; Data S1). Importantly, the ribosome-associated protein AT5G24490, homologous to spinach PSRP1/pY, was found to be highly enriched at 144k (Data S1). This suggests that a proportion of TM-associated ribosomes are inactivated under the light conditions used in this work (Sharma et al., 2010).

PSII repair cycle-associated components

After PSII photodamage in the grana core, the complex undergoes monomerization and gains access to the non-appressed TM regions (SEM) to replace the damaged D1 protein, starting with D1 dephosphorylation and degradation (Järvi et al., 2015). However, the two classes of proteases synergistically involved in D1 degradation (Kato et al., 2012) were differentially segregated upon TM fractionation. The TM-spanning FTSH heterocomplex, composed of type A (FTSH1/5) and type B (FTSH2/8) isomers (Zhang et al., 2010), was found to be enriched in both CD (40k) and SL (144k), whereas the soluble DEG proteases accumulated in the LP fraction, providing another example of the heterogeneity of the LP fraction. DEG1 and DEG5/8, which cleave the C-D TMD lumenal loop and DEG7, which cleaves the D-E stromal loop, generate more N-termini for the progressive protease activity of FTSH (Table 1) (Kato & Sakamoto, 2014). The coiled-coil protein THF1 was also enriched with FSTH in the CD (40k). THF1 has been shown to interact with FTSH in Synechocystis by pull-down assays (Bečková et al., 2017), which is consistent with the Arabidopsis *thf1* mutant showing low levels of FTSH5 as well as FTSH2 (Zhang et al., 2009; Zhu et al., 2020). Furthermore, the knock-out mutants of *ftsh2* and *fsth5* (but not *ftsh1* and *ftsh8*), as well as of *thf1*, show a variegated phenotype (Chen et al., 2000; Zhang et al., 2010). Taken together, these results suggest a strong interaction between FSTH and THF1 in the degradation of D1 in the 40k CD, whereas the soluble DEG proteases, which *in vivo* cooperate with the FTSH proteases, are released into the LP fraction during TM fractionation.

D1 translation initiation

After D1 degradation, a newly synthetized D1 precursor (pD1) is inserted into the CP43-less complex before the CP43 module is reassociated (Järvi et al., 2015; Nickelsen & Rengstl, 2013; Theis & Schroda, 2016). Translation of D1, the protein with the highest turnover in the TM, involves CP33B and CP33C, which stabilize the *PsbA* mRNA, and the SDR protein HCF173, all of which are enriched in 40k CD and 144k SL (Table 1). HCF173 is responsible for tethering *psbA* mRNA-loaded ribosomes to the TM. This occurs before the insertion of the first D1 TMD into the ALB3-cpSECY translocase channel (see below) (Klostermann et al., 2002; Link et al., 2012; Schult et al., 2007; Zhang et al., 2001). The N-terminus of D1 is then processed by the PEPTIDE DEFORMYLASE 1B, which is associated with the nascent D1 chain (Dirk et al., 2002; Stolle et al., 2024) and is also enriched in 40k CD and 144k (Table 1).

pD1 insertion into TM occurs in a specific lipid microenvironment

The co-translational insertion and folding of D1 into TM requires the formation of a highly enriched PG environment in all photosynthetic organisms (Nordhues et al., 2012; Theis & Schroda, 2016; Yoshihara & Kobayashi, 2022). PG is the least abundant glycerolipid in the TM (Garab et al., 2022) and accumulates around the cpSEC1 translocase, similar to cardiolipin (CL) in the bacterial SECYEG complex, for stability and activation (Akopian et al., 2013; Gold et al., 2010; Walter et al., 2015). The cpSEC1 translocation pathway consists of two membrane-spanning components that form narrow channels for unfolded protein insertion into the TM (SCY1 and SECE1) and a stromal component, SECA1, all of which accumulate in the LP and, to a lesser extent, in 144k (Table 1). However, for co-translational insertion, SCY1 forms also a stable complex with the insertase ALB3, enriched at 144k, similar to that observed in bacteria (Klostermann et al., 2002).

The observed discrepancy in the localization of D1 insertion and the translocase pathways, upon TM fractionation, may be explained in terms of lipid microenvironments in the TM. A PG-enriched microdomain, together with a weak interaction of DIG with PG (Orczyk et al., 2017) (see discussion above), leads to poor solubilization by DIG of the translocone complex formed by ALB3 and the ALB3-associated pool of SCY1, which consequently accumulate in the 40k and 144k vesicle fractions (Table 1; Figure 7). Thus, the dual localization of the cpSEC1 pathway in 40k and in 144k as well as in LP might indicate where the translocone complex is recruited to be activated by the anionic lipid environment for D1 insertion (Akopian et al., 2013). This is consistent with the co-localization of part of cpSEC1 with ALB3 and the entire translation machinery (ribosomes, HCF173, etc., see above), and also with the strong co-enrichment of a third membrane protein, TERC, involved in cpSEC1-ALB3-dependent D1 insertion (Table 1) (Schneider et al., 2014). However, the bacterial SECYEG translocase is also stimulated by non-bilayer lipids (van der Does et al., 2000), so the pool of cpSEC1 segregating into the LP could be the one involved in the translocation of proteins other than D1, that is, with less PG requirement. Two other proteins, PAM68 (a linker between PSII and ribosomes; Armbruster et al., 2010) and PSBN, which help to fold and assemble the PSII reaction center (RC) proteins D1 and D2 into larger complexes during PSII biogenesis and repair (Järvi et al., 2015; Lu, 2016), are also enriched in the 40k and 144k fractions, respectively. Thus, the co-translational insertion of D1 takes place in the CD (40k) and SL (144k).

In general, the accumulation of PSII monomer and CP43-less in the LP, together with several auxiliary proteins involved in PSII repair, may indicate that part of the steps of the repair cycle are separated into the LP due to the specific lipid environment, as discussed above. Recent literature points to the importance of specific lipids associated with PSII for proper folding and function (Magyar

et al., 2024), and further experimental work is needed to clarify this point in the context of PSII biogenesis and repair cycle.

CONCLUSIONS

The CURT1-containing curvature domain (in LP) cannot be purified by using detergents for solubilization and subsequent fractionation of the TM. This is probably due to the interaction of specific annular lipids of various TM proteins and protein complexes (Cyt b_6f, ATP synthase, PSII monomer) with the saponin used for TM fractionation, causing them to accumulate in the LP fraction together with the true curvature proteins, the CURT1 proteins. The highly curved curvature domains, formed by specific features of the CURT1-type proteins, which have been studied in a number of different biological membranes, are generally unable to accommodate large protein complexes. Translated to the TM, the curvature domains can only form at the outer edges of the grana discs and at specific sites of the stroma thylakoids (Figure 1). Instead, the grana margin connecting domain (CD), defined as an intermediate domain directly connecting the appressed grana and non-appressed stroma membranes, is enriched in the 40k fraction. The CD domain is characterized by the PSI-LHCII state-transition complex, the presence of LHCII and the NDH-1 complex as well as a number of PSII assembly proteins together with the translation machinery. We provide the proteome map of the fractions enriched in grana core (10k), CD (40k) and SL (144k), as well as the LP fraction containing the curvature, plastoglobuli and several proteins and protein complexes solubilized in small vesicles by DIG. This map, together with the optimized protocol described for obtaining the fractions, is a powerful tool for meta-analysis of the TM proteins of interest to the plant science community.

MATERIALS AND METHODS

Plant growth, thylakoid isolation and fractionation

To understand how the solubilization with digitonin (DIG) affects the distribution of the thylakoid protein complexes in fractions collected at increasing centrifugation speed, an experimental procedure described in Figure 1(a) has been set up. Plant growth, thylakoid isolation and fractionation were performed as in Trotta et al. (2019) with slight modifications. Plants of wild-type Arabidopsis (*Arabidopsis thaliana*) ecotype Col-0 were grown in phytotron under 120 μmol photons m^{-2} sec^{-1} (8 h light/16 h dark) using OSRAM PowerStar (Munich, Germany) HQIT 400/D Metal Halide lamps as the light source at 25°C for 32 days. TMs were isolated in dim light at 4°C from fresh whole rosettes collected 2 h after the onset of the light period and ground in ice-cold buffer containing 50 mM Tricine/NaOH (pH 7.8), 400 mM sorbitol, 10 mM NaCl, 5 mM $MgCl_2$ and 10 mM NaF. After filtration through two layers of Miracloth, thylakoids were pelleted at 2739 ***g*** at 4°C for 5 min, resuspended in a shock buffer (15 mM Tricine/NaOH [pH 7.8], 10 mM NaCl, 5 mM $MgCl_2$ and 10 mM NaF) and centrifuged again at 630 ***g*** at 4°C for 5 min. Thylakoids were washed with resuspension buffer (15 mM Tricine/KOH [pH 7.8], 100 mM sorbitol, 10 mM NaCl, 5 mM $MgCl_2$ and 10 mM NaF), centrifuged at 630 ***g***, and finally resuspended in the same buffer = resuspension buffer.

Next, TMs were washed six times in either presence (stacked) or absence (linearized) of $MgCl_2$. The two preparations were subjected to solubilization with [DIG] corresponding to 0.1% w/v (0.8 mM), 0.25% (2 mM) or 0.4% (3.2 mM) as in Trotta et al. (2019). The details about the fractionation procedure, gel electrophoresis and immunoblotting, 77 K fluorescence measurements and TEM are provided in Data S3.

Mass spectrometry analysis and protein quantification

Intact stacked thylakoids and the 10k, 40k, 144k and LP fractions obtained after solubilization with 0.25% DIG have been processed for tryptic digestion as described in (Gollan et al., 2021; Trotta et al., 2019). Analysis by liquid-chromatography electrospray-ionization MS/MS was performed as in (Gollan et al., 2021; Trotta et al., 2019), except that a Q-Exactive HF electrospray ionization-hybrid quadrupole-orbitrap mass spectrometer (Thermo Fisher Scientific) was used, the scan range was 300 to 1800 *m/z*, with up to 15 data-dependent MS/MS spectra acquired in each scan and dynamic exclusion set for 30 sec. The acquired MS/MS spectra have been analyzed as described in Trotta et al. (2019) except that Proteome Discover v2.4 (PD v2.4; Thermo Fisher Scientific, Waltham, Massachusetts, USA) was used for label-free protein quantification with Data Dependent Acquisition (DDA). For protein quantification, intact thylakoids were set as control and the protein abundances were calculated as percentage of the control ($n = 3$). The PD v2.4 settings used for protein quantification are reported in Data S1.

AUTHOR CONTRIBUTIONS

AT designed the research, performed research, analyzed data, wrote the paper; SG performed research, analyzed data, wrote the paper; AAB performed research, analyzed data; VP designed the research, performed research, analyzed data; HF performed research, analyzed data; E-MA designed the research, analyzed data, wrote the paper.

ACKNOWLEDGMENTS

The authors thank Marjaana Rantala for fruitful discussions and Ilaria Mancini for her excellent technical assistance in gel electrophoresis. The authors thank the Biocenter Finland and the Proteomics Facility of the Turku Centre for Biotechnology for their excellent support in the MS and TEM analyses. Research was financially supported by the Jane and Aatos Erkko Foundation.

CONFLICT OF INTEREST

The authors declare no conflict of interest.

DATA AVAILABILITY STATEMENT

The mass spectrometry proteomics data have been deposited to the ProteomeXchange Consortium (http://proteomecentral.proteomexchange.org) via the PRIDE partner repository (Perez-Riverol et al., 2022) with the dataset identifier PXD046544 and DOI: 10.6019/PXD046544.

SUPPORTING INFORMATION

Additional Supporting Information may be found in the online version of this article.

Figure S1. Pictures of the supernatants and pellets collected during fractionation.

Figure S2. 2D-lpBN/SDS-PAGE of thylakoids and conventional fractions collected from stacked TM.

Figure S3. 2D-lpBN/SDS-PAGE, lpBN-PAGE and SDS-PAGE of the fractions collected from linearized TM.

Figure S4. Particle size distribution in the fractions obtained with 0.25% DIG from stacked and linearized TM analyzed by TEM.

Figure S5. Analysis of the LP and the other fractions collected after solubilization with different [DIG].

Figure S6. Cyt b6f and PSII monomer are easily solubilized from thylakoids by DIG.

Figure S7. 2D-lpBN/SDS-PAGE of 144k and LP with or without solubilization with β-DM or DIG prior loading on lpBN-PAGE.

Figure S8. Segregation of CURT1, Cyt b_6f and PSII monomer in LP independently of the centrifugation speed to collect the LP fractions.

Figure S9. Protein composition of the major clusters from the heat map in Figure 6(b).

Data S1. List of proteins identified by mass spectrometry and sorting of the plastidial proteins in categories.

Data S2. Locus identifiers and gene symbols of the proteins in Figure 7.

Data S3. Supplementary materials and methods.

REFERENCES

Akopian, D., **Shen, K.**, **Zhang, X.** & **Shan, S.** (2013) Signal recognition particle: an essential protein-targeting machine. *Annual Review of Biochemistry*, **82**, 693–721.

Albertsson, P.-Å., **Andreasson, E.**, **Svensson, P.** & **Yu, S.-G.** (1991) Localization of cytochrome f in the thylakoid membrane: evidence for multiple domains. *Biochimica et Biophysica Acta (BBA) - Bioenergetics*, **1098**, 90–94.

Anderson, J.M. (2012) Lateral heterogeneity of plant thylakoid protein complexes: early reminiscences. *Philosophical Transactions of the Royal Society, B: Biological Sciences*, **367**, 3384–3388.

Anderson, J.M. & **Boardman, N.K.** (1966) Fractionation of the photochemical systems of photosynthesis I. Chlorophyll contents and photochemical activities of particles isolated from spinach chloroplasts. *Biochimica et Biophysica Acta (BBA) - Biophysics including Photosynthesis*, **112**, 403–421.

Anderson, J.M., **Horton, P.**, **Kim, E.-H.** & **Chow, W.S.** (2012) Towards elucidation of dynamic structural changes of plant thylakoid architecture. *Philosophical Transactions of the Royal Society, B: Biological Sciences*, **367**, 3515–3524.

Anderson, J.M. & **Vernon, L.P.** (1967) Digitonin incubation of spinach chloroplasts in tris (hydroxymethyl) methylglycine solutions of varying ionic strengths. *Biochimica et Biophysica Acta (BBA) - Bioenergetics*, **143**, 363–376.

Andersson, B. & **Anderson, J.M.** (1980) Lateral heterogeneity in the distribution of chlorophyll-protein complexes of the thylakoid membranes of spinach chloroplasts. *Biochimica et Biophysica Acta (BBA) - Bioenergetics*, **593**, 427–440.

Armbruster, U., **Labs, M.**, **Pribil, M.**, **Viola, S.**, **Xu, W.**, **Scharfenberg, M.** ***et al.*** (2013) Arabidopsis CURVATURE THYLAKOID1 proteins modify THYLAKOID architecture by inducing membrane curvature. *Plant Cell*, **25**, 2661–2678. Available from: https://doi.org/10.1105/tpc.113.113118

Armbruster, U., **Zühlke, J.**, **Rengstl, B.**, **Kreller, R.**, **Makarenko, E.**, **Rühle, T.** ***et al.*** (2010) The *Arabidopsis* thylakoid protein PAM68 is required for efficient D1 biogenesis and photosystem II assembly. *Plant Cell*, **22**, 3439–3460.

Aro, E.-M., **Suorsa, M.**, **Rokka, A.**, **Allahverdiyeva, Y.**, **Paakkarinen, V.**, **Saleem, A.** ***et al.*** (2005) Dynamics of photosystem II: a proteomic approach to thylakoid protein complexes. *Journal of Experimental Botany*, **56**, 347–356.

Augustin, J.M., **Kuzina, V.**, **Andersen, S.B.** & **Bak, S.** (2011) Molecular activities, biosynthesis and evolution of triterpenoid saponins. *Phytochemistry*, **72**, 435–457.

Bečková, M., **Yu, J.**, **Krynická, V.**, **Kozlo, A.**, **Shao, S.**, **Koník, P.** ***et al.*** (2017) Structure of Psb29/Thf1 and its association with the FtsH protease complex involved in photosystem II repair in cyanobacteria. *Philosophical Transactions of the Royal Society, B: Biological Sciences*, **372**, 20160394.

Bell, A.J., **Frankel, L.K.** & **Bricker, T.M.** (2015) High yield non-detergent isolation of photosystem I-light-harvesting chlorophyll II membranes from spinach thylakoids: implications for the organization of the PS I antennae in higher plants. *The Journal of Biological Chemistry*, **290**, 18429–18437.

Benz, M., **Bals, T.**, **Gügel, I.L.**, **Piotrowski, M.**, **Kuhn, A.**, **Schünemann, D.** ***et al.*** (2009) Alb4 of Arabidopsis promotes assembly and stabilization of a non chlorophyll-binding photosynthetic complex, the CF1CF0–ATP synthase. *Molecular Plant*, **2**, 1410–1424.

Bussi, Y., **Shimoni, E.**, **Weiner, A.**, **Kapon, R.**, **Charuvi, D.**, **Nevo, R.** ***et al.*** (2019) Fundamental helical geometry consolidates the plant photosynthetic membrane. *Proceedings of the National Academy of Sciences of the United States of America*, **116**, 22366–22375.

Caffarri, S., **Kouril, R.**, **Kereïche, S.**, **Boekema, E.J.** & **Croce, R.** (2009) Functional architecture of higher plant photosystem II supercomplexes. *The EMBO Journal*, **28**, 3052–3063.

Chen, M., **Choi, Y.**, **Voytas, D.F.** & **Rodermel, S.** (2000) Mutations in the Arabidopsis VAR2 locus cause leaf variegation due to the loss of a chloroplast FtsH protease. *The Plant Journal*, **22**, 303–313.

Cramer, W.A. (2019) Structure–function of the cytochrome b6f lipoprotein complex: a scientific odyssey and personal perspective. *Photosynthesis Research*, **139**, 53–65.

Danielsson, R. & **Albertsson, P.-Å.** (2009) Fragmentation and separation analysis of the photosynthetic membrane from spinach. *Biochimica et Biophysica Acta (BBA) - Bioenergetics*, **1787**, 25–36.

Danielsson, R., **Suorsa, M.**, **Paakkarinen, V.**, **Albertsson, P.-A.Å.**, **Styring, S.**, **Aro, E.-M.M.** ***et al.*** (2006) Dimeric and monomeric organization of photosystem II: distribution of five distinct complexes in the different domains of the thylakoid membrane. *Journal of Biological Chemistry*, **281**, 14241–14249.

Daum, B. & **Kuhlbrandt, W.** (2011) Electron tomography of plant thylakoid membranes. *Journal of Experimental Botany*, **62**, 2393–2402.

Daum, B., **Nicastro, D.**, **Austin, J.**, **McIntosh, J.R.** & **Kühlbrandt, W.** (2010) Arrangement of photosystem II and ATP synthase in chloroplast membranes of spinach and pea. *Plant Cell*, **22**, 1299–1312.

Dekker, J.P. & **Boekema, E.J.** (2005) Supramolecular organization of thylakoid membrane proteins in green plants. *Biochimica et Biophysica Acta (BBA) - Bioenergetics*, **1706**, 12–39.

Dirk, L.M.A., **Williams, M.A.** & **Houtz, R.L.** (2002) Specificity of chloroplast-localized peptide deformylases as determined with peptide analogs of chloroplast-translated proteins. *Archives of Biochemistry and Biophysics*, **406**, 135–141.

Dlouhý, O., **Karlický, V.**, **Arshad, R.**, **Zsiros, O.**, **Domonkos, I.**, **Kurasová, I.** ***et al.*** (2021) Lipid polymorphism of the subchloroplast—granum and stroma thylakoid membrane–particles. II. Structure and functions. *Cells*, **10**, 2363.

Dlouhý, O., **Kurasová, I.**, **Karlický, V.**, **Javornik, U.**, **Šket, P.**, **Petrova, N.Z.** ***et al.*** (2020) Modulation of non-bilayer lipid phases and the structure and functions of thylakoid membranes: effects on the water-soluble enzyme violaxanthin de-epoxidase. *Scientific Reports*, **10**, 11959.

Duchêne, S. & **Siegenthaler, P.** (2000) Do glycerolipids display lateral heterogeneity in the thylakoid membrane? *Lipids*, **35**, 739–744.

Dunahay, T.G., **Staehelin, L.A.**, **Seibert, M.**, **Ogilvie, P.D.** & **Berg, S.P.** (1984) Structural, biochemical and biophysical characterization of four oxygen-evolving photosystem II preparations from spinach. *Biochimica et Biophysica Acta (BBA) - Bioenergetics*, **764**, 179–193.

Fan, H.Y., **Das, D.** & **Heerklotz, H.** (2016) "Staying out" rather than "cracking in": asymmetric membrane insertion of 12:0 Lysophosphocholine. *Langmuir*, **32**, 11655–11663.

Fan, H.Y. & **Heerklotz, H.** (2017) Digitonin does not flip across cholesterol-poor membranes. *Journal of Colloid and Interface Science*, **504**, 283–293.

Garab, G., **Yaguzhinsky, L.S.**, **Dlouhý, O.**, **Nesterov, S.V.**, **Špunda, V.** & **Gasanoff, E.S.** (2022) Structural and functional roles of non-bilayer lipid phases of chloroplast thylakoid membranes and mitochondrial inner membranes. *Progress in Lipid Research*, **86**, 101163.

Garcia, M., **Myouga, F.**, **Takechi, K.**, **Sato, H.**, **Nabeshima, K.**, **Nagata, N.** ***et al.*** (2007) An Arabidopsis homolog of the bacterial peptidoglycan synthesis enzyme MurE has an essential role in chloroplast development. *The Plant Journal*, **53**, 924–934.

Gerotto, C., **Trotta, A.**, **Bajwa, A.A.**, **Mancini, I.**, **Morosinotto, T.** & **Aro, E.-M.** (2019) Thylakoid protein phosphorylation dynamics in a moss mutant lacking SERINE/THREONINE PROTEIN KINASE STN8. *Plant Physiology*, **180**, 1582–1597.

Giménez-Andrés, M., **Čopič, A.** & **Antonny, B.** (2018) The many faces of amphipathic helices. *Biomolecules*, **8**, 45.

Gold, V.A.M., **Robson, A.**, **Bao, H.**, **Romantsov, T.**, **Duong, F.** & **Collinson, I.** (2010) The action of cardiolipin on the bacterial translocon. *Proceedings of the National Academy of Sciences of the United States of America*, **107**, 10044–10049.

Gollan, P.J., **Trotta, A.**, **Bajwa, A.A.**, **Mancini, I.** & **Aro, E.** (2021) Characterization of the free and membrane-associated fractions of the thylakoid lumen proteome in *Arabidopsis thaliana*. *International Journal of Molecular Sciences*, **22**, 8126.

Graça, A.T., **Hall, M.**, **Persson, K.** & **Schröder, W.P.** (2021) High-resolution model of Arabidopsis photosystem II reveals the structural consequences of digitonin-extraction. *Scientific Reports*, **11**, 15534.

Grebe, S., **Trotta, A.**, **Bajwa, A.A.**, **Suorsa, M.**, **Gollan, P.J.**, **Jansson, S.** ***et al.*** (2019) The unique photosynthetic apparatus of Pinaceae: analysis of photosynthetic complexes in *Picea abies*. *Journal of Experimental Botany*, **70**, 3211–3225.

Grieco, M., **Suorsa, M.**, **Jajoo, A.**, **Tikkanen, M.** & **Aro, E.-M.** (2015) Light-harvesting II antenna trimers connect energetically the entire photosynthetic machinery—including both photosystems II and I. *Biochimica et Biophysica Acta (BBA) - Bioenergetics*, **1847**, 607–619.

Gupta, T.K., **Klumpe, S.**, **Gries, K.**, **Heinz, S.**, **Wietrzynski, W.**, **Ohnishi, N.** ***et al.*** (2021) Structural basis for VIPP1 oligomerization and maintenance of thylakoid membrane integrity. *Cell*, **184**, 3643–3659.e23.

Hurt, E. & **Hauska, G.** (1981) A cytochrome f/b6 complex of five polypeptides with plastoquinol-plastocyanin-oxidoreductase activity from spinach chloroplasts. *European Journal of Biochemistry*, **117**, 591–595.

Järvi, S., **Suorsa, M.** & **Aro, E.-M.** (2015) Photosystem II repair in plant chloroplasts—regulation, assisting proteins and shared components with photosystem II biogenesis. *Biochimica et Biophysica Acta (BBA) - Bioenergetics*, **1847**, 900–909. Available from: https://doi.org/10.1016/j.bbabio.2015.01.006

Järvi, S., **Suorsa, M.**, **Paakkarinen, V.** & **Aro, E.-M.** (2011) Optimized native gel systems for separation of thylakoid protein complexes: novel super- and mega-complexes. *Biochemical Journal*, **439**, 207–214. Available from: https://doi.org/10.1042/BJ20102155

Jeon, Y., **Jung, H.J.**, **Kang, H.**, **Park, Y.**, **Lee, S.H.** & **Pai, H.** (2012) S1 domain-containing STF modulates plastid transcription and chloroplast biogenesis in *Nicotiana benthamiana*. *New Phytologist*, **193**, 349–363.

Jimbo, H. & **Wada, H.** (2023) Deacylation of galactolipids decomposes photosystem II dimers to enhance degradation of damaged D1 protein. *Plant Physiology*, **191**, 87–95.

Johnson, M.P., **Vasilev, C.**, **Olsen, J.D.** & **Hunter, C.N.** (2014) Nanodomains of cytochrome b6f and photosystem II complexes in spinach grana thylakoid membranes. *Plant Cell*, **26**, 3051–3061.

Kato, Y. & **Sakamoto, W.** (2014) Phosphorylation of photosystem II core proteins prevents undesirable cleavage of D1 and contributes to the fine-tuned repair of photosystem II. *The Plant Journal*, **79**, 312–321.

Kato, Y., **Sun, X.**, **Zhang, L.** & **Sakamoto, W.** (2012) Cooperative D1 degradation in the photosystem II repair mediated by chloroplastic proteases in Arabidopsis. *Plant Physiology*, **159**, 1428–1439.

Kettunen, R., **Lehtonen, E.**, **Tyystjärvi, E.** & **Aro, E.** (1992) Degradation products of the D1 protein are located in the non-appressed regions of the thylakoid membrane in vivo. In *Research in photosynthesis. Volume IV Proceedings of the IXth International Congress on Photosynthesis*, Nagoya, Japan, August 30–September 4, 1992. pp. 309–316.

Klostermann, E., **Droste Gen Helling, I.**, **Carde, J.-P.** & **Schünemann, D.** (2002) The thylakoid membrane protein ALB3 associates with the cpSecY-translocase in *Arabidopsis thaliana*. *Biochemical Journal*, **368**, 777–781.

Kobayashi, K., **Endo, K.** & **Wada, H.** (2017) Specific distribution of phosphatidylglycerol to photosystem complexes in the thylakoid membrane. *Frontiers in Plant Science*, **8**, 1–7.

Könnel, A., **Bugaeva, W.**, **Gügel, I.L.** & **Philippar, K.** (2019) BANFF: bending of bilayer membranes by a mphiphilic α-helices is necessary for form and function of organelles. *Biochemistry and Cell Biology*, **97**, 243–256.

Koochak, H., **Puthiyaveetil, S.**, **Mullendore, D.L.**, **Li, M.** & **Kirchhoff, H.** (2019) The structural and functional domains of plant thylakoid membranes. *The Plant Journal*, **97**, 412–429. Available from: https://doi.org/10.1111/tpj.14127

Korotych, O., **Mondal, J.**, **Gattás-Asfura, K.M.**, **Hendricks, J.** & **Bruce, B.D.** (2019) Evaluation of commercially available styrene-co-maleic acid polymers for the extraction of membrane proteins from spinach chloroplast thylakoids. *European Polymer Journal*, **114**, 485–500.

Korotych, O.I., **Nguyen, T.T.**, **Reagan, B.C.**, **Burch-Smith, T.M.** & **Bruce, B.D.** (2021) Poly(styrene-co-maleic acid)-mediated isolation of supramolecular membrane protein complexes from plant thylakoids. *Biochimica et Biophysica Acta (BBA) - Bioenergetics*, **1862**, 148347.

Kouřil, R., **Wientjes, E.**, **Bultema, J.B.**, **Croce, R.** & **Boekema, E.J.** (2013) High-light vs. low-light: effect of light acclimation on photosystem II composition and organization in *Arabidopsis thaliana*. *Biochimica et Biophysica Acta - Bioenergetics*, **1827**, 411–419.

Kruse, O., **Hankamer, B.**, **Konczak, C.**, **Gerle, C.**, **Morris, E.**, **Radunz, A.** ***et al.*** (2000) Phosphatidylglycerol is involved in the dimerization of photosystem II. *Journal of Biological Chemistry*, **275**, 6509–6514.

Kyle, D.J., **Kuang, T.**, **Watson, J.L.** & **Arntzen, C.J.** (1984) Movement of a sub-population of the light harvesting complex (LHCII) from grana to stroma lamellae as a consequence of its phosphorylation. *Biochimica et Biophysica Acta (BBA) - Bioenergetics*, **765**, 89–96.

Link, S., **Engelmann, K.**, **Meierhoff, K.** & **Westhoff, P.** (2012) The atypical short-chain dehydrogenases HCF173 and HCF244 are jointly involved in translational initiation of the psbA mRNA of Arabidopsis. *Plant Physiology*, **160**, 2202–2218.

Lu, Y. (2016) Identification and roles of photosystem II assembly, stability, and repair factors in Arabidopsis. *Frontiers in Plant Science*, **7**, 168. Available from: https://doi.org/10.3389/fpls.2016.00168

Maeda, H., **Takahashi, K.**, **Ueno, Y.**, **Sakata, K.**, **Yokoyama, A.**, **Yarimizu, K.** ***et al.*** (2022) Characterization of photosystem II assembly complexes containing ONE-HELIX PROTEIN1 in *Arabidopsis thaliana*. *Journal of Plant Research*, **135**, 361–376.

Magyar, M., **Akhtar, P.**, **Sipka, G.**, **Domonkos, I.**, **Han, W.**, **Li, X.** ***et al.*** (2024) Effects of lipids on the rate-limiting steps in the dark-to-light transition of photosystem II core complex of *Thermostichus vulcanus*. *Frontiers in Plant Science*, **15**, 1040. Available from: https://doi.org/10.3389/fpls.2024.1381040/full

Mazur, R., **Mostowska, A.** & **Kowalewska, Ł.** (2021) How to measure grana – ultrastructural features of thylakoid membranes of plant chloroplasts. *Frontiers in Plant Science*, **12**, 756009.

Meng, L., **Du, M.**, **Zhu, T.**, **Li, G.**, **Ding, Y.** & **Zhang, Q.** (2024) PPR proteins in plants: roles, mechanisms, and prospects for rice research. *Frontiers in Plant Science*, **15**, 6742. Available from: https://doi.org/10.3389/fpls.2024.1416742/full

Mohamed, A., **Nishi, S.**, **Kawakami, K.**, **Shen, J.-R.**, **Itoh, S.**, **Fukumura, H.** ***et al.*** (2022) Exciton quenching by oxidized chlorophyll Z across the two adjacent monomers in a photosystem II core dimer. *Photosynthesis Research*, **154**, 277–289.

Murphy, D.J. (1982) The importance of non-planar bilayer regions in photosynthetic membranes and their stabilisation by galactolipids. *FEBS Letters*, **150**, 19–26.

Murphy, D.J. (1986) The molecular organisation of the photosynthetic membranes of higher plants. *Biochimica et Biophysica Acta (BBA) - Reviews on Biomembranes*, **864**, 33–94.

Nelson, N. & **Neumann, J.** (1972) Isolation of a cytochrome b6-f Particle from chloroplasts. *Journal of Biological Chemistry*, **247**, 1817–1824.

Nickelsen, J. & **Rengstl, B.** (2013) Photosystem II assembly: from cyanobacteria to plants. *Annual Review of Plant Biology*, **64**, 609–635. Available from: https://doi.org/10.1146/annurev-arplant-050312-120124

Nishikawa, M., **Nojima, S.**, **Akiyama, T.**, **Sankawa, U.** & **Inoue, K.** (1984) Interaction of digitonin and its analogs with membrane cholesterol. *Journal of Biochemistry*, **96**, 1231–1239.
Nishimura, K., **Kato, Y.** & **Sakamoto, W.** (2017) Essentials of proteolytic machineries in chloroplasts. *Molecular Plant*, **10**, 4–19.
Nishioka, K., **Kato, Y.**, **Ozawa, S.**, **Takahashi, Y.** & **Sakamoto, W.** (2021) Phos-tag-based approach to study protein phosphorylation in the thylakoid membrane. *Photosynthesis Research*, **147**, 107–124.
Nordhues, A., **Schöttler, M.A.**, **Unger, A.-K.**, **Geimer, S.**, **Schönfelder, S.**, **Schmollinger, S.** ***et al.*** (2012) Evidence for a role of VIPP1 in the structural organization of the photosynthetic apparatus in *Chlamydomonas*. *Plant Cell*, **24**, 637–659.
Olinares, P.D.B., **Ponnala, L.** & **Van Wijk, K.J.** (2010) Megadalton complexes in the chloroplast stroma of *Arabidopsis thaliana* characterized by size exclusion chromatography, mass spectrometry, and hierarchical clustering. *Molecular & Cellular Proteomics*, **9**, 1594–1615.
Orczyk, M., **Wojciechowski, K.** & **Brezesinski, G.** (2017) Disordering effects of digitonin on phospholipid monolayers. *Langmuir*, **33**, 3871–3881.
Pàli, T., **Garab, G.**, **Horváth, L.I.** & **Kóta, Z.** (2003) Functional significance of the lipid-protein interface in photosynthetic membranes. *Cellular and Molecular Life Sciences*, **60**, 1591–1606.
Peng, L., **Fukao, Y.**, **Fujiwara, M.**, **Takami, T.** & **Shikanai, T.** (2009) Efficient operation of NAD(P)H dehydrogenase requires supercomplex formation with photosystem I via minor LHCI in Arabidopsis. *Plant Cell*, **21**, 3623–3640.
Perez-Riverol, Y., **Bai, J.**, **Bandla, C.**, **García-Seisdedos, D.**, **Hewapathirana, S.**, **Kamatchinathan, S.** ***et al.*** (2022) The PRIDE database resources in 2022: a hub for mass spectrometry-based proteomics evidences. *Nucleic Acids Research*, **50**, D543–D552.
Phan, M.D., **Korotych, O.I.**, **Brady, N.G.**, **Davis, M.M.**, **Satija, S.K.**, **Ankner, J.F.** ***et al.*** (2020) X-ray and neutron reflectivity studies of styrene-maleic acid copolymer interactions with galactolipid-containing monolayers. *Langmuir*, **36**, 3970–3980.
Pick, U. & **Racker, E.** (1979) Purification and reconstitution of the N,N′-dicyclohexylcarbodiimide-sensitive ATPase complex from spinach chloroplasts. *Journal of Biological Chemistry*, **254**, 2793–2799.
Puthiyaveetil, S., **Tsabari, O.**, **Lowry, T.**, **Lenhert, S.**, **Lewis, R.R.**, **Reich, Z.** ***et al.*** (2014) Compartmentalization of the protein repair machinery in photosynthetic membranes. *Proceedings of the National Academy of Sciences of the United States of America*, **111**, 15839–15844.
Rantala, M., **Rantala, S.** & **Aro, E.-M.** (2020) Composition, phosphorylation and dynamic organization of photosynthetic protein complexes in plant thylakoid membrane. *Photochemical & Photobiological Sciences*, **19**, 604–619.
Rantala, S. & **Tikkanen, M.** (2018) Phosphorylation-induced lateral rearrangements of thylakoid protein complexes upon light acclimation. *Plant Direct*, **2**, e00039.
Raven, J.A. (2021) Determinants, and implications, of the shape and size of thylakoids and cristae. *Journal of Plant Physiology*, **257**, 153342.
Rochaix, J.-D., **Lemeille, S.**, **Shapiguzov, A.**, **Samol, I.**, **Fucile, G.**, **Willig, A.** ***et al.*** (2012) Protein kinases and phosphatases involved in the acclimation of the photosynthetic apparatus to a changing light environment. *Philosophical Transactions of the Royal Society, B: Biological Sciences*, **367**, 3466–3474. Available from: https://doi.org/10.1098/rstb.2012.0064
Romanowska, E. & **Albertsson, P.-Å.** (1994) Isolation and characterization of the cytochrome bf complex from whole thylakoids, grana, and stroma lamellae vesicles from spinach chloroplasts. *Plant & Cell Physiology*, **35**, 557–568.
Scheidelaar, S., **Koorengevel, M.C.**, **Pardo, J.D.**, **Meeldijk, J.D.**, **Breukink, E.** & **Killian, J.A.** (2015) Molecular model for the solubilization of membranes into nanodisks by styrene maleic acid copolymers. *Biophysical Journal*, **108**, 279–290.
Schneider, A., **Steinberger, I.**, **Strissel, H.**, **Kunz, H.H.**, **Manavski, N.**, **Meurer, J.** ***et al.*** (2014) The Arabidopsis tellurite resistance C protein together with ALB3 is involved in photosystem II protein synthesis. *Plant Journal*, **78**, 344–356.
Schölz, C., **Parcej, D.**, **Ejsing, C.S.**, **Robenek, H.**, **Urbatsch, I.L.** & **Tampé, R.** (2011) Specific lipids modulate the transporter associated with antigen processing (TAP). *Journal of Biological Chemistry*, **286**, 13346–13356.
Schult, K., **Meierhoff, K.**, **Paradies, S.**, **Töller, T.**, **Wolff, P.** & **Westhoff, P.** (2007) The nuclear-encoded factor HCF173 is involved in the initiation of translation of the psbA mRNA in *Arabidopsis thaliana*. *Plant Cell*, **19**, 1329–1346.
Seiwert, D., **Witt, H.**, **Janshoff, A.** & **Paulsen, H.** (2017) The non-bilayer lipid MGDG stabilizes the major light-harvesting complex (LHCII) against unfolding. *Scientific Reports*, **7**, 5158.
Sharma, M.R., **Dönhöfer, A.**, **Barat, C.**, **Marquez, V.**, **Datta, P.P.**, **Fucini, P.** ***et al.*** (2010) PSRP1 is not a ribosomal protein, but a ribosome-binding Factor that is recycled by the ribosome-recycling Factor (RRF) and elongation Factor G (EF-G). *Journal of Biological Chemistry*, **285**, 4006–4014.
Shen, L., **Tang, K.**, **Wang, W.**, **Wang, C.**, **Wu, H.**, **Mao, Z.** ***et al.*** (2021) Architecture of the chloroplast PSI-NDH supercomplex in *Hordeum vulgare*. *Nature*, **601**, 649–654.
Simidjiev, I., **Stoylova, S.**, **Amenitsch, H.**, **Jávorfi, T.**, **Mustárdy, L.**, **Laggner, P.** ***et al.*** (2000) Self-assembly of large, ordered lamellae from non-bilayer lipids and integral membrane proteins in vitro. *Proceedings of the National Academy of Sciences of the United States of America*, **97**, 1473–1476.
Smith, E.L. (1988) The discovery of chlorophyll-protein complex by Emil L. Smith during 1937–1941. *Photosynthesis Research*, **16**, 285–289.
Stolle, D.S., **Osterhoff, L.**, **Treimer, P.**, **Lambertz, J.**, **Karstens, M.**, **Keller, J.M.** ***et al.*** (2024) STIC2 selectively binds ribosome-nascent chain complexes in the cotranslational sorting of Arabidopsis thylakoid proteins. *The EMBO Journal*, **43**, 4699–4719. Available from: https://doi.org/10.1038/s44318-024-00211-4
Su, X., **Cao, D.**, **Pan, X.**, **Shi, L.**, **Liu, Z.**, **Dall'Osto, L.** ***et al.*** (2022) Supramolecular assembly of chloroplast NADH dehydrogenase-like complex with photosystem I from *Arabidopsis thaliana*. *Molecular Plant*, **15**, 454–467.
Sudji, I., **Subburaj, Y.**, **Frenkel, N.**, **García-Sáez, A.** & **Wink, M.** (2015) Membrane disintegration caused by the steroid saponin digitonin is related to the presence of cholesterol. *Molecules*, **20**, 20146–20160.
Suorsa, M., **Rantala, M.**, **Mamedov, F.**, **Lespinasse, M.**, **Trotta, A.**, **Grieco, M.** ***et al.*** (2015) Light acclimation involves dynamic re-organization of the pigment-protein megacomplexes in non-appressed thylakoid domains. *The Plant Journal*, **84**, 360–373. Available from: https://doi.org/10.1111/tpj.13004
Swainsbury, D.J.K., **Proctor, M.S.**, **Hitchcock, A.**, **Cartron, M.L.**, **Qian, P.**, **Martin, E.C.** ***et al.*** (2018) Probing the local lipid environment of the cytochrome bc1 and Synechocystis sp. PCC 6803 cytochrome b6f complexes with styrene maleic acid. *Biochimica et Biophysica Acta (BBA) - Bioenergetics*, **1859**, 215–225.
Thalhammer, A. & **Hincha, D.K.** (2014) A mechanistic model of COR15 protein function in plant freezing tolerance: integration of structural and functional characteristics. *Plant Signaling & Behavior*, **9**, e977722.
Theis, J. & **Schroda, M.** (2016) Revisiting the photosystem II repair cycle. *Plant Signaling & Behavior*, **11**, e1218587. Available from: https://doi.org/10.1080/15592324.2016.1218587
Tikkanen, M., **Nurmi, M.**, **Suorsa, M.**, **Danielsson, R.**, **Mamedov, F.**, **Styring, S.** ***et al.*** (2008) Phosphorylation-dependent regulation of excitation energy distribution between the two photosystems in higher plants. *Biochimica et Biophysica Acta (BBA) - Bioenergetics*, **1777**, 425–432.
Tomizioli, M., **Lazar, C.**, **Brugière, S.**, **Burger, T.**, **Salvi, D.**, **Gatto, L.** ***et al.*** (2014) Deciphering thylakoid sub-compartments using a mass spectrometry-based approach. *Molecular & Cellular Proteomics*, **13**, 2147–2167.
Tremmel, I.G., **Kirchhoff, H.**, **Weis, E.** & **Farquhar, G.D.** (2003) Dependence of plastoquinol diffusion on the shape, size, and density of integral thylakoid proteins. *Biochimica et Biophysica Acta (BBA) - Bioenergetics*, **1607**, 97–109.
Trotta, A., **Bajwa, A.A.**, **Mancini, I.**, **Paakkarinen, V.**, **Pribil, M.** & **Aro, E.-M.** (2019) The role of phosphorylation dynamics of curvature thylakoid 1B in plant thylakoid membranes. *Plant Physiology*, **181**, 1615–1631.
van der Does, C., **Swaving, J.**, **van Klompenburg, W.** & **Driessen, A.J.M.** (2000) Non-bilayer lipids stimulate the activity of the reconstituted bacterial protein translocase. *Journal of Biological Chemistry*, **275**, 2472–2478.
van der Weij-de Wit, C.D., **Ihalainen, J.A.**, **van Grondelle, R.** & **Dekker, J.P.** (2007) Excitation energy transfer in native and unstacked thylakoid membranes studied by low temperature and ultrafast fluorescence spectroscopy. *Photosynthesis Research*, **93**, 173–182.
Van Eerden, F.J., **De Jong, D.H.**, **De Vries, A.H.**, **Wassenaar, T.A.** & **Marrink, S.J.** (2015) Characterization of thylakoid lipid membranes from cyanobacteria and higher plants by molecular dynamics simulations. *Biochimica et Biophysica Acta (BBA) - Biomembranes*, **1848**, 1319–1330.

Van Roon, H., **Van Breemen, J.F.L.**, **De Weerd, F.L.**, **Dekker, J.P.** & **Boekema, E.J.** (2000) Solubilization of green plant thylakoid membranes with n-dodecyl-alpha,D-maltoside. Implications for the structural organization of the photosystem II, photosystem I, ATP synthase and cytochrome b6 f complexes. *Photosynthesis Research*, **64**, 155–166.

Walter, B., **Hristou, A.**, **Nowaczyk, M.M.** & **Schünemann, D.** (2015) In vitro reconstitution of co-translational D1 insertion reveals a role of the cpSec–Alb3 translocase and Vipp1 in photosystem II biogenesis. *Biochemical Journal*, **468**, 315–324.

Wang, L., **Leister, D.** & **Kleine, T.** (2020) Chloroplast development and genomes uncoupled signaling are independent of the RNA-directed DNA methylation pathway. *Scientific Reports*, **10**, 15412. Available from: https://doi.org/10.1038/s41598-020-71907-w

Wang, P. & **Grimm, B.** (2021) Connecting chlorophyll metabolism with accumulation of the photosynthetic apparatus. *Trends in Plant Science*, **26**, 484–495.

Watkins, K.P., **Williams-Carrier, R.**, **Chotewutmontri, P.**, **Friso, G.**, **Teubner, M.**, **Belcher, S.** ***et al.*** (2020) Exploring the proteome associated with the mRNA encoding the D1 reaction center protein of photosystem II in plant chloroplasts. *The Plant Journal*, **102**, 369–382.

Wittig, I. & **Schägger, H.** (2005) Advantages and limitations of clear-native PAGE. *Proteomics*, **5**, 4338–4346.

Wojciechowski, K., **Orczyk, M.**, **Gutberlet, T.**, **Brezesinski, G.**, **Geue, T.** & **Fontaine, P.** (2016) On the interaction between digitonin and cholesterol in Langmuir monolayers. *Langmuir*, **32**, 9064–9073.

Wollenberger, L., **Stefansson, H.**, **Yu, S.-G.** & **Albertsson, P.-Å.** (1994) Isolation and characterization of vesicles originating from the chloroplast grana margins. *Biochimica et Biophysica Acta (BBA) - Bioenergetics*, **1184**, 93–102.

Wu, X.-X., **Mu, W.-H.**, **Li, F.**, **Sun, S.-Y.**, **Cui, C.-J.**, **Kim, C.** ***et al.*** (2024) Cryo-EM structures of the plant plastid-encoded RNA polymerase. *Cell*, **187**, 1127–1144.e21. Available from: https://doi.org/10.1016/j.cell.2024.01.026

Yamamoto, T., **Burke, J.**, **Autz, G.** & **Jagendorf, A.T.** (1981) Bound ribosomes of pea chloroplast thylakoid membranes: location and release in vitro by high Salt, puromycin, and RNase. *Plant Physiology*, **67**, 940–949.

Yoshihara, A. & **Kobayashi, K.** (2022) Lipids in photosynthetic protein complexes in the thylakoid membrane of plants, algae, and cyanobacteria. *Journal of Experimental Botany*, **73**, 2735–2750.

Zhang, D., **Kato, Y.**, **Zhang, L.**, **Fujimoto, M.**, **Tsutsumi, N.**, **Sodmergen** et al. (2010) The FtsH protease heterocomplex in Arabidopsis: dispensability of type-B protease activity for proper chloroplast development. *Plant Cell*, **22**, 3710–3725.

Zhang, L., **Kato, Y.**, **Otters, S.**, **Vothknecht, U.C.** & **Sakamoto, W.** (2012) Essential role of VIPP1 in chloroplast envelope maintenance in Arabidopsis. *Plant Cell*, **24**, 3695–3707.

Zhang, L., **Paakkarinen, V.**, **Suorsa, M.** & **Aro, E.-M.** (2001) A SecY homologue is involved in chloroplast-encoded D1 protein biogenesis. *Journal of Biological Chemistry*, **276**, 37809–37814.

Zhang, L., **Paakkarinen, V.**, **van Wijk, K.J.** & **Aro, E.-M.** (2000) Biogenesis of the chloroplast-encoded D1 protein: regulation of translation elongation, insertion, and assembly into photosystem II. *Plant Cell*, **12**, 1769–1781.

Zhang, L., **Wei, Q.**, **Wu, W.**, **Cheng, Y.**, **Hu, G.**, **Hu, F.** ***et al.*** (2009) Activation of the heterotrimeric G protein α-subunit GPA1 suppresses the ftsh-mediated inhibition of chloroplast development in Arabidopsis. *The Plant Journal*, **58**, 1041–1053.

Zhu, Y., **Wu, W.**, **Shao, W.**, **Chen, J.**, **Shi, X.**, **Ma, X.** ***et al.*** (2020) SPLICING FACTOR1 is important in chloroplast development under cold stress. *Plant Physiology*, **184**, 973–987.